Geosci. Model Dev., 10, 453–482, 2017
www.geosci-model-dev.net/10/453/2017/
doi:10.5194/gmd-10-453-2017

Geoscientific Model Development
Open Access
EGU

Bottom RedOx Model (BROM v.1.1): a coupled benthic–pelagic model for simulation of water and sediment biogeochemistry

Evgeniy V. Yakushev[1,2], Elizaveta A. Protsenko[1,2], Jorn Bruggeman[3], Philip Wallhead[4], Svetlana V. Pakhomova[5,2,7], Shamil Kh. Yakubov[2], Richard G. J. Bellerby[6,4], and Raoul-Marie Couture[1,8]

[1]Norwegian Institute for Water Research (NIVA), Gaustadalléen 21, 0349 Oslo, Norway
[2]P.P. Shirshov Institute of Oceanology RAS, Nakhimovskiy prosp. 36, 117991, Moscow, Russia
[3]Plymouth Marine Laboratory, Prospect Place, The Hoe, Plymouth, PL1 3DH, UK
[4]Norwegian Institute for Water Research (NIVA Vest), Thormøhlensgate 53 D, 5006 Bergen, Norway
[5]Norwegian Institute for Air Research (NILU), P.O. Box 100, 2027 Kjeller, Norway
[6]State Key Laboratory for Estuarine and Coastal Research, East China Normal University, Shanghai, China
[7]Norwegian University of Science and Technology (NTNU), 7491 Trondheim, Norway
[8]University of Waterloo, Earth and Environmental Sciences, Ecohydrology Group,
200 University Avenue West, N2L3G2, Waterloo, Canada

Correspondence to: Evgeniy V. Yakushev (evgeniy.yakushev@niva.no)

Received: 29 October 2015 – Published in Geosci. Model Dev. Discuss.: 15 January 2016
Revised: 17 November 2016 – Accepted: 13 December 2016 – Published: 1 February 2017

Abstract. Interactions between seawater and benthic systems play an important role in global biogeochemical cycling. Benthic fluxes of some chemical elements (e.g., C, N, P, O, Si, Fe, Mn, S) alter the redox state and marine carbonate system (i.e., pH and carbonate saturation state), which in turn modulate the functioning of benthic and pelagic ecosystems. The redox state of the near-bottom layer in many regions can change with time, responding to the supply of organic matter, physical regime, and coastal discharge. We developed a model (BROM) to represent key biogeochemical processes in the water and sediments and to simulate changes occurring in the bottom boundary layer. BROM consists of a transport module (BROM-transport) and several biogeochemical modules that are fully compatible with the Framework for the Aquatic Biogeochemical Models, allowing independent coupling to hydrophysical models in 1-D, 2-D, or 3-D. We demonstrate that BROM is capable of simulating the seasonality in production and mineralization of organic matter as well as the mixing that leads to variations in redox conditions. BROM can be used for analyzing and interpreting data on sediment–water exchange, and for simulating the consequences of forcings such as climate change, external nutrient loading, ocean acidification, carbon storage leakage, and point-source metal pollution.

1 Background

Oxygen depletion and anoxia are increasingly common phenomena observed in the World Ocean, inland seas, and coastal areas. Observations show a decline in dissolved oxygen concentrations at continental margins in many regions, and this has been linked to both an increase in anthropogenic nutrient loadings and a decrease in vertical mixing (e.g., Diaz and Rosenberg, 2008; Rabalais et al., 2002; Richardson and Jørgensen, 1996). Although bottom waters may be permanently oxic or anoxic, they oscillate seasonally between these extremes in many water bodies (Morse and Eldridge, 2007). Such oscillations typically result from variations in the supply of organic matter (OM) to the sediment–water interface (SWI), from the hydrophysical regime (mixing/ventilation), and from nutrient supply (river runoff). Frequently, oxic conditions during periods of intense mixing are followed by near-bottom suboxia or anoxia after the seasonal pycnocline forms, restricting aeration of the deeper layers. This occurs, for instance, on the Louisiana shelf (Morse and Eldridge, 2007; Yu et al., 2015) and in Corpus Christi Bay (McCarthy et al., 2008), the Sea of Azov (Debolskaya et al., 2008), and Eleusis Bay (Pavlidou et al., 2013).

The redox state and oxygenation of near-bottom water varies due to the transport of oxidized and reduced species across the SWI and biogeochemical processes occurring in the sediments (Cooper and Morse, 1996; Jorgensen et al., 1990; Roden and Tuttle, 1992; Sell and Morse, 2006). The sediments generally consume oxygen due to the deposition of labile OM and the presence of reduced forms of chemical elements. Their capacity to exchange oxygen with the pelagic layer is limited, as near-bottom water is usually characterized by low water velocity and reduced mixing in the vicinity of the SWI (Glud, 2008). In some cases, a high benthic oxygen demand (BOD) associated with local OM mineralization and low mixing rates can cause anoxia in the bottom water. This may lead to death, migration, or changed behavior of the benthic macro- and meiofaunal organisms responsible for bioturbation and bioirrigation (Blackwelder et al., 1996; Sen Gupta et al., 1996; Morse and Eldridge, 2007), which in turn can greatly slow down the transport of solid and dissolved species inside the sediments and therefore the rates of oxidative reactions. Under such conditions, sedimentary sulfides can build up, and dissolution of carbonate minerals may come to a halt (Morse and Eldridge, 2007). When oxic conditions return, there can be an "oxygen debt" of reduced species in the water column (Yakushev et al., 2011) which may buffer and delay reoxygenation of the sediments (Morse and Eldridge, 2007).

In areas experiencing seasonal hypoxia/anoxia, the processes taking place in the water column and in the sediments are tightly coupled to each other, as well as to the fluxes and exchanges of organic matter over a range of timescales. An accurate understanding of physical, chemical, and biological processes driving changes in redox conditions is needed to predict the distribution of hypoxia/anoxia in a given environment. This "benthic–pelagic coupling" broadly encompasses the fluxes of OM to the sediments and the return fluxes of inorganic nutrients to the water column. Variations in supply, dynamics, and reactivity of OM affect benthic communities (Pearson and Rosenberg, 1978), sediment and porewater geochemistry (Berner, 1980), and nutrient and oxygen fluxes at the SWI (Boudreau, 1997).

Many previous studies have demonstrated the capability of sophisticated reactive transport codes for integrated modeling of biogeochemical cycles in sediments (Boudreau, 1996; Van Cappellen and Wang, 1996; Couture et al., 2010; Jourabchi et al., 2005; Katsev et al., 2006, 2007; Paraska et al., 2014; Soetaert et al., 1996). The water column redox interface was also specifically targeted in the models of Konovalov et al. (2006) and Yakushev et al. (2006, 2007, 2011). However, the process of integrating such models with pelagic biogeochemical models to produce benthic–pelagic coupled models has only begun in recent years.

As of the year 2000, benthic–pelagic coupling was either neglected or crudely approximated in many pelagic biogeochemical and early diagenetic models (Soetaert et al., 2000). One of the first fully coupled physical–pelagic–benthic biogeochemical modes was developed for the Goban Spur shelf break area to examine the impact of in situ atmospheric conditions on ecosystem dynamics, to understand biogeochemical distributions in the water column and the sediments, and to derive a nitrogen budget for the area. This model was most suited for testing the impact of short-term physical forcing on the ecosystem (Soetaert et al., 2001).

Later, several coupled benthic–pelagic models were produced with an emphasis on studying eutrophication (Cerco et al., 2006; Fennel et al., 2011; Soetaert and Middelburg, 2009) or hypoxia in various locations including Tokyo Bay (Sohma et al., 2008), the Baltic Sea (Reed et al., 2011), the North Sea oyster grounds (Meire et al., 2013), and the Southern Bight (Lancelot et al., 2005). Another model was created to investigate early diagenesis of silica in the Scheldt estuary, with benthic–pelagic coupling only of silica (Arndt and Regnier, 2007).

By coupling two quite sophisticated models ECOHAM1 and C.CANDI, a 3-D model for the North Sea was created where pelagic model output was used to force a benthic biogeochemical module (Luff and Moll, 2004). Another physical–biological model for the North Sea, PROWQM, is more complex than ECOHAM1 and has been coupled to a benthic module to simulate seasonal changes of chlorophyll, nutrients, and oxygen at the PROVESS north site, southeast of the Shetland Islands (Lee et al., 2002). Brigolin et al. (2011) developed a spatially explicit model for the northwestern Adriatic coastal zone by coupling a 1-D transient early diagenesis model with a 2-D reaction-transport pelagic biogeochemical model. Currently, the most known and established coupled model is ERSEM – the European Regional Seas Ecosystem Model, which was initially developed as a coastal ecosystem model for the North Sea and which has evolved into a generic tool for ecosystem simulations from shelf seas to the global ocean (Butenschön et al., 2016).

The BROM model described herein is a fully coupled benthic–pelagic model with a special focus on deoxygenation and redox biogeochemistry in the sediments and benthic boundary layer (BBL). The BBL is "the part of the marine environment that is directly influenced by the presence of the interface between the bed and its overlying water" (Dade et al., 2001). Physical scientists tend to prefer the term "bottom boundary layer", but this is largely synonymous with the BBL (Thorpe, 2005). Within BROM, the term BBL refers to the lower parts of the fluid bottom boundary layer where bottom friction strongly inhibits current speed and vertical mixing, hence including the viscous and logarithmic sublayers up to at most a few meters above the sediment. This calm-water layer plays a critical role in mediating the interaction of the water column and sediment biogeochemistry and in determining, e.g., near-bottom oxygen levels, yet it remains poorly resolved in most physical circulation models. For BROM, we have developed an accompanying offline transport module (BROM-transport) that uses output from hydrodynamic water column models but solves the transport-

reaction equations for a "full" grid including both water column and sediments. BROM-transport uses greatly increased spatial resolution near the SWI, and thereby provides explicit spatial resolution of the BBL and sediments.

The goal of this work was to develop a model that captures key biogeochemical processes in the water and sediment and to analyze the changes occurring in the BBL and SWI. As a result, BROM differs from existing biogeochemical models in several key respects. BROM features explicit, detailed descriptions of many chemical transformations under different redox conditions, and tracks the fate of several chemical elements (Mn, Fe, and S) and compounds ($MnCO_3$, FeS, S^0, S_2O_3) that rarely appear in other models. BROM also allows for spatially explicit representations of the vertical structure in the sediments and BBL. This distinguishes it from, e.g., ERSEM (Butenschön et al., 2016), which has a more detailed representation of larger benthic organisms (meiofauna and different types of macrofauna), but limits its chemistry to the dissolved phase to CO_2, O_2, and macronutrients, its benthic bacteria to two functional groups, and its sedimentary vertical structure to an implicit three-layer representation that relies on equilibrium profiles of solutes and idealized profiles of particulates. Third, BROM offers a near-comprehensive representation of all processes affecting oxygen levels in the BBL and sediments, and should therefore provide a useful tool for studies focused on deoxygenation in deep water and sediments. Finally, BROM is designed as a flexible model that can be applied in a broad range of marine and lake environments and modeling problems. As a component of the Framework for Aquatic Biogeochemical Modeling (FABM; Bruggeman and Bolding, 2014), BROM can be very easily coupled online to any hydrodynamic model within FABM, and can also be driven offline by hydrodynamic model output saved in NetCDF or text format using the purpose-built offline transport solver BROM-transport.

2 BROM description

BROM consists of two modules, BROM-biogeochemistry and BROM-transport. BROM-biogeochemistry builds on ROLM (RedOx Layer Model), a model constructed to simulate basic biogeochemical structure of the water column oxic/anoxic interface in the Black Sea, Baltic Sea, and Norwegian fjords (He et al., 2012; Stanev et al., 2014; Yakushev et al., 2009, 2006, 2007, 2011). In BROM-biogeochemistry, we extended the list of modeled compounds and processes (Fig. 1). BROM considers interconnected transformations of species of N, P, Si, C, O, S, Mn, and Fe, and resolves OM in nitrogen currency. OM dynamics include parameterizations of OM production (via photosynthesis and chemosynthesis) and OM decay via oxic mineralization, denitrification, metal reduction, sulfate reduction, and methanogenesis. To provide a detailed representation of changing redox conditions, OM in BROM is mineralized by several different electron acceptors and dissolved oxygen is consumed during both mineralization of OM and oxidation of various reduced compounds. Process inhibition in accordance with redox potential is parameterized by various redox-dependent switches. BROM also includes a module describing the carbonate equilibria; this allows BROM to be used to investigate acidification and impacts of changing pH and saturation states on water and sediment biogeochemistry.

The physical domain of BROM-transport spans the water column, BBL, and upper layers of the sediments in a continuous fashion. This allows for an explicit, high-resolution representation of the BBL and upper sediments, while also allowing the boundary conditions to be moved as far as possible from these foci of interest, i.e., to the air–sea interface and to deep in the sediment.

BROM is integrated into an existing modular platform (FABM) and is therefore coded as a set of reusable "LEGO brick" components, including the offline transport driver BROM-transport and modules for ecology, redox chemistry, and carbonate chemistry. This means that BROM-transport can be used with all biogeochemical modules available in FABM, including, e.g., the modules comprising ERSEM, and that BROM biogeochemical modules can be used in all other 1-D and 3-D hydrodynamic models supported by FABM (e.g., GOTM, GETM, MOM5, NEMO, FVCOM). Individual BROM modules can also be coupled to existing ecological models to expand their scope, e.g., by providing descriptions of redox and carbonate chemistry. Using the FABM framework thus facilitates the transparent and consistent setup of complex biogeochemical reaction networks for the prediction of hypoxia/anoxia while harnessing the capabilities of various hydrophysical drivers.

2.1 Biogeochemical module

2.1.1 General description

BROM-biogeochemistry consists of three biogeochemical submodules: BROM_bio (ecological model), BROM_redox (redox processes), and BROM_carb (carbonate system). Interactions between modeled variables are either kinetic (e.g., OM degradation) or equilibrium processes (e.g., carbonate system equilibration) (Boudreau, 1996; Jourabchi et al., 2008; Luff et al., 2001). In general, the redox reactions are fast in comparison with the other processes and a typical model time step. Species involved in such reactions are therefore set to equilibrium concentrations using mass action laws and equilibrium constants for seawater (Millero, 1995). Total scale pH is also diagnosed at every time step, mainly as a function of dissolved inorganic carbon (DIC) and total alkalinity (Alk) which are both prognostic (state) variables.

The model has 33 state variables (Table 1), including frequently measured components such as hydrogen sulfide (H_2S) and phosphate (PO_4), as well as rarely measured variables such as elemental sulfur (S^0), thiosulfate (S_2O_3), triva-

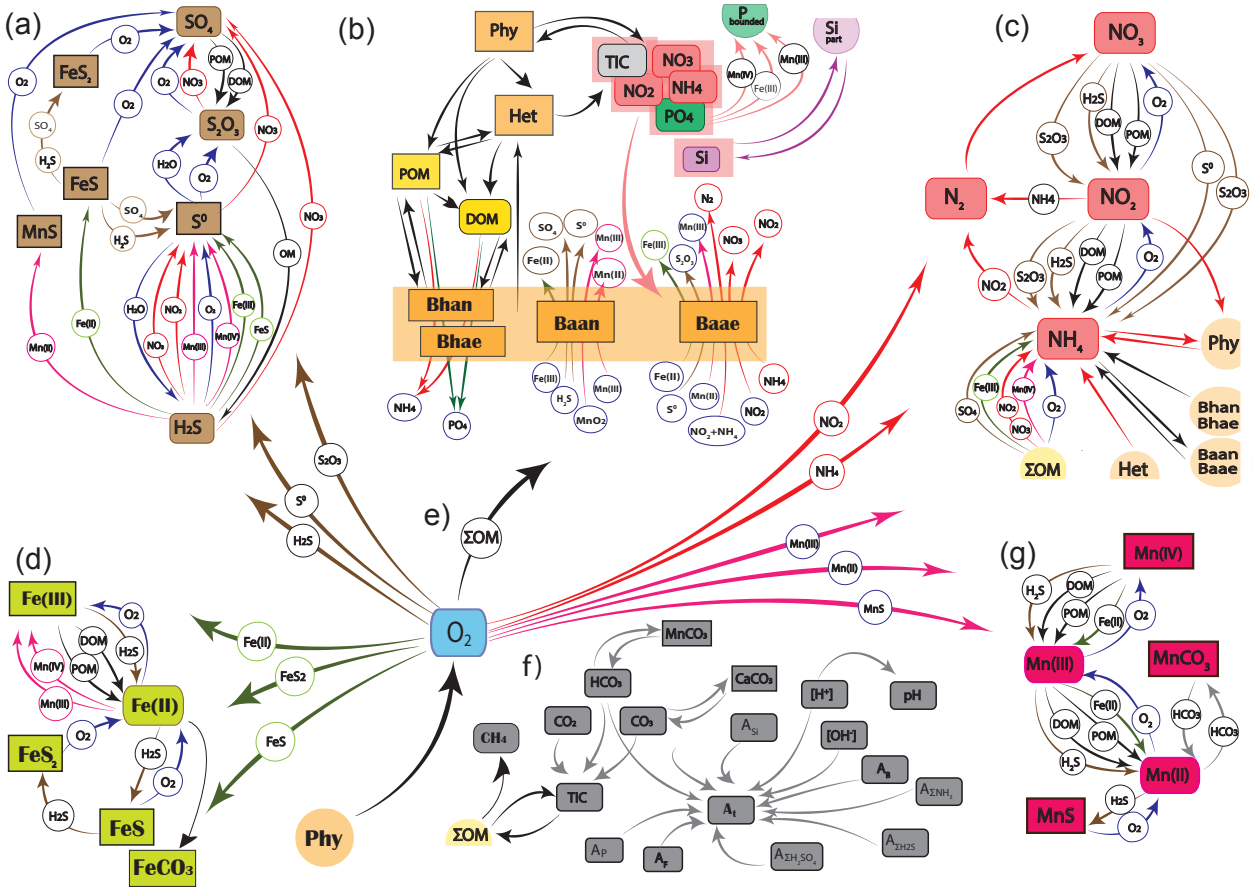

Figure 1. Flow chart of biogeochemical processes represented in the Benthic RedOx Model (BROM), showing the transformation of sulfur species **(a)**, the ecological block **(b)**, the transformation of nitrogen species **(c)**, the transformation of iron species **(d)**, the processes affecting dissolved oxygen **(e)**, the carbonate system and alkalinity **(f)**, and the transformation of manganese species **(g)**.

lent manganese species Mn(III), and bacteria. We acknowledge that for many of these, site-specific estimates of associated model parameters and initial/boundary conditions may be difficult or impossible to obtain, and may in practice require some crude assumptions and approximations (e.g., universal default parameter values, no-flux boundary conditions, and initial conditions from a steady annual cycle). Nevertheless, we believe that for many applications this caveat will be acceptable given the additional process resolution and realism provided by BROM for important biogeochemical processes in the BBL and sediments. The equations and parameters employed in BROM are given in Tables 2 and 3, and a flow chart is shown in Fig. 1.

2.1.2 Ecosystem and redox models

The overall goal of the ecosystem representation is to parameterize the key features of OM production and decomposition, following Redfield and Richards stoichiometry (Richards, 1965). We divide all the living OM (biota) into Phy (photosynthetic biota), Het (non-microbial heterotrophic biota), and four groups of "bacteria" which may be considered to include microbial fungi. These latter are Baae (aerobic chemoautotrophic bacteria), Baan (anaerobic chemoautotrophic bacteria), Bhae (aerobic heterotrophic bacteria), and Bhan (anaerobic heterotrophic bacteria). OM is produced photosynthetically by Phy and chemosynthetically by bacteria, specifically by Baae in oxic conditions and by Baan in anoxic conditions. Growth of heterotrophic bacteria is tied to mineralization of OM, favoring Bhae in oxic conditions and Bhan in anoxic conditions. Secondary production is represented by Het, which consumes phytoplankton as well as all types of bacteria and dead particulate organic matter (detritus, which is also explicitly modeled). The effect of suboxia and anoxia is parameterized by letting the mortality of aerobic organisms depend on the oxygen availability.

A detailed account of processes representing the inorganic cycling of N, S, Mn, Fe, and P is given in the description of ROLM (Yakushev et al., 2007, 2013a), while the process parameterization, chemical reactions, rates, and stoichiometric constants values are summarized in Tables 2–4. Table 2 also describes the redox-dependent switches, nutrient

Table 1. State variables of BROM.

No.	Notation	Name	Units	No.	Notation	Name	Units
	N	Nitrogen			O	Oxygen	
1	NH_4	Ammonia	µM N	19	O_2	Dissolved oxygen	µM O_2
2	NO_2	Nitrite	µM N		S	Sulfur	
3	NO_3	Nitrate	µM N	20	H_2S	Hydrogen sulfide	µM S
4	PON	Particulate organic nitrogen	µM N	21	S^0	Total elemental sulfur	µM S
5	DON	Dissolved organic nitrogen	µM N	22	S_2O_3	Thiosulfate and sulfites	µM S
	P	Phosphorus		23	SO_4	Sulfate	µM S
6	PO_4	Phosphate	µM P		C	Carbon	
	Si	Silicon		24	DIC	Dissolved inorganic carbon	µM C
7	Si	Dissolved silicon	µM Si	25	CH_4	Methane	µM C
8	Si_part	Particulate silicon	µM Si	26	$CaCO_3$	Calcium carbonate	µM Ca
	Mn	Manganese				Alkalinity	
9	Mn^{2+}	Dissolved bivalent manganese	µM Mn	27	Alk	Total alkalinity	µM
10	Mn^{3+}	Dissolved trivalent manganese	µM Mn				
11	Mn^{4+}	Particulate quadrivalent manganese	µM Mn			Ecosystem parameters	
12	MnS	Manganese sulfide	µM Mn	28	Phy	Phototrophic producers	µM N
13	$MnCO_3$	Manganese carbonate	µM Mn	29	Het	Pelagic and benthic heterotrophs	µM N
	Fe	Iron		30	Bhae	Aerobic heterotrophic bacteria	µM N
14	Fe^{2+}	Dissolved bivalent iron	µM Fe	31	Baae	Aerobic autotrophic bacteria	µM N
15	Fe^{3+}	Particulate trivalent iron	µM Fe	32	Bhan	Anaerobic heterotrophic bacteria	µM N
16	FeS	Iron monosulfide	µM Fe	33	Baan	Anaerobic autotrophic bacteria	µM N
17	FeS_2	Pyrite	µM Fe				
18	$FeCO_3$	Ferrous Carbonate	µM Fe				

limitation, and substrate consumption rates for heterotrophs. The redox-dependent switches are mostly based on hyperbolic tangent functions which improve system stability compared with discrete switches. The nutrient limitation and heterotrophic transfer functions are based on squared Monod laws for nutrient–biomass ratio, which also stabilizes the system compared with Michaelis–Menten and Ivlev formulations. Here, we describe the parameterization of carbon that was not considered in ROLM and was not described in Yakushev (2013).

2.1.3 Total alkalinity

Total alkalinity, A_T, is a model state variable. Following the formal definition of A_T (Dickson, 1992; Wolf-Gladrow et al., 2007; Zeebe and Wolf-Gladrow, 2001), the following alkalinity components were considered:

$$A_T = A_{TCO2} + A_B + A_{TPO4} + A_{Si} + A_{NH3} + A_{H2S} + [OH^-] - A_{SO4} - A_{HF} - A_{HNO3} - [H^+],$$

where the carbonate alkalinity ($A_{TCO2} = [HCO_3^-] + 2[CO_3^{2-}]$), phosphoric alkalinity ($A_{TPO4} = [HPO_4^{2-}] + 2[PO_4^{3-}] - [H_3PO_4]$), silicic alkalinity ($A_{Si} = [H_3SiO_4^-]$), ammonia alkalinity ($A_{NH3} = [NH_3]$), and hydrogen sulfide alkalinity ($A_{H2S} = [HS^-]$) were calculated from the corresponding model state variables (Table 1) according to Luff et al. (2001) and Volkov (1984). The boric alkalinity $A_B = [B(OH)_4^-]$ was estimated from total dissolved boron, which in turn was calculated from salinity. $[OH^-]$ and $[H^+]$ were calculated using the ion product of water (Millero, 1995). The hydrogen sulfate alkalinity ($A_{SO4} = [HSO_4^-]$), hydrofluoric alkalinity ($A_{HF} = [HF]$), and nitrous acid alkalinity ($A_{HNO3} = [HNO_2]$) were ignored due to their insignificant impact on A_T variations in most natural marine and freshwater systems.

Biogeochemical processes can lead to either increase or decrease of alkalinity, and alkalinity can be used as an indicator of specific biogeochemical processes (Soetaert et al., 2007). Organic matter production can affect alkalinity via the "nutrient-H^+ compensating principle" formulated by Wolf-Gladrow et al. (2007): during uptake or release of charged nutrient species, electroneutrality is maintained by consumption or production of a proton (i.e., during uptake of nitrate for photosynthesis or denitrification, or production of nitrate by nitrification).

BROM also considers the effect on alkalinity of the following redox reactions occurring in suboxic and anoxic conditions via production or consumption of $[OH^-]$ and $[H^+]$ and changes in other "standard" alkalinity components A_{TCO2} and A_{H2S} (see bold font):

$$4Mn^{2+} + O_2 + \mathbf{4H^+} \rightarrow 4Mn^{3+} + 2H_2O$$
$$2Mn^{3+} + 3H_2O + 0.5O_2 \rightarrow 2MnO_2 + \mathbf{6H^+}$$
$$2MnO_2 + \mathbf{7H^+} + \mathbf{HS^-} \rightarrow 2Mn^{3+} + 4H_2O + S^0$$

Table 2. Parameterization of the biogeochemical processes: **(a)** nutrients; **(b)** redox metals and sulfur; **(c)** carbon and alkalinity; **(d)** ecosystem processes.

(a)	
Name of process, reference, reaction	Parameterization in the model
	Nitrogen
Autolysis (Savchuk and Wulff, 1996)	Autolysis = K_PON_DON × **PON**
Mineralization at oxic conditions (Richards, 1965) $(CH_2O)_{106}(NH_3)_{16}H_3PO_4 + 106O_2 \rightarrow$ $106CO_2 + 16NH_3 + H_3PO_4 + 106H_2O$	DcDM_O2=K_DON_ox × **DON** × $\frac{\mathbf{O_2}}{\mathbf{O_2}+\text{K\_omox\_o2}} \times (1 + \text{beta\_da}\frac{t^2}{t^2+tda^2})$ DcPM_O2=K_PON_ox × **PON** × $\frac{\mathbf{O_2}}{\mathbf{O_2}+\text{K\_omox\_o2}} \times (1 + \text{beta\_da}\frac{t^2}{t^2+tda^2})$
Nitrification stage 1 (Canfield et al., 2005): $NH_4^+ + 1.5O_2 \rightarrow NO_2^- + 2H^+ + H_2O$ Nitrification stage 2 (Canfield et al., 2005): $NO_2^- + 0.5\,O_2 \rightarrow NO_3^-$	Nitrif1 = K_nitrif1 × $\mathbf{NH_4}$ × $\mathbf{O_2}$ × 0.5× (1.0 + tanh ($\mathbf{O_2}$ − O2s_nf)) Nitrif2 = K_nitrif2 × $\mathbf{NO_2}$ × $\mathbf{O_2}$ × 0.5× (1.0 + tanh ($\mathbf{O_2}$ − O2s_nf))
Anammox (Canfield et al., 2005): $NO_2^- + NH_4^+ \rightarrow N_2 + 2H_2O$	Anammox = K_anammox × $\mathbf{NO_2}$ × $\mathbf{NH_4}$ × (1 − 0.5 × (1 + tanh ($\mathbf{O_2}$ − O2s_dn)))
POM denitrification 1st stage: (Anderson et al., 1982) $0.5CH_2O + NO_3^- \rightarrow NO_2^- + 0.5H_2O + 0.5CO_2$ 2nd stage: (Anderson et al., 1982) $0.75CH_2O + H^+ + NO_2^- \rightarrow 0.5N_2 + 1.25H_2O + 0.75CO_2$	Denitr1_PM = K_denitr1 × F_dnox × $\frac{\mathbf{NO_3}}{\mathbf{NO_3}+\text{K\_ommo\_no3}}$ × **PON** Denitr2_PM = K_denitr2 × F_dnox × $\frac{\mathbf{NO_2}}{\mathbf{NO_2}+\text{K\_ommo\_no2}}$ × **PON** where F_dnox=1 − 0.5 × (1 + tanh ($\mathbf{O_2}$ − O2s_dn)) DcPM_NOX = $\frac{16}{212}$ × Denitr1_PM + $\frac{16}{141.3}$ × Denitr2_PM
DOM denitrification (Anderson et al., 1982)	Denitr1_DM = K_denitr1 × F_dnox × $\frac{\mathbf{NO_3}}{\mathbf{NO_3}+\text{K\_ommo\_no3}}$ × **DON** Denitr2_DM = K_denitr2 × F_dnox × $\frac{\mathbf{NO_2}}{\mathbf{NO_2}+\text{K\_ommo\_no3}}$ × **DON** where F_dnox = 1 − 0.5 × (1 + tanh ($\mathbf{O_2}$ − O2s_dn)) DcDM_NOX = $\frac{16}{212}$ × Denitr1_DM + $\frac{16}{141.3}$ × Denitr2_DM
	Phosphate
Complexation with Mn(III) (Yakushev et al., 2007): Complexation with Fe(III) (Yakushev et al., 2007):	mn_p_compl = (mn_ox2+mn_rd2-mn_ox1-mn_rd1)/ r_mn_p fe_p_compl = (fe_rd-fe_ox1-fe_ox2 + 4. × DcDM_Fe + 4. × DcPM_Fe)/r_fe_p
	Silicate
Dissolution of particulate Si (Popova and Srokosz, 2009): Complexation with Fe(III):	sipartdiss = **Si**_part × K_sipart_diss fe_si_compl = (fe_rd-fe_ox1-fe_ox2+4. × DcDM_Fe + 4. × DcPM_Fe)/r_fe_si

$2Mn^{3+} + \mathbf{HS^-} \rightarrow 2Mn^{2+} + S^0 + \mathbf{H^+}$

$Mn^{2+} + \mathbf{HS^-} \leftrightarrow MnS + \mathbf{H^+}$

$Mn^{2+} + \mathbf{CO_3^{2-}} \leftrightarrow MnCO_3$

$2MnCO_3 + O_2 + 2H_2O \rightarrow 2MnO_2 + \mathbf{2HCO_3^-} + \mathbf{2H^+}$

$4Fe^{2+} + O_2 + 10H_2O \rightarrow 4Fe(OH)_3 + \mathbf{8H^+}$

$2Fe^{2+} + MnO_2 + 4H_2O \rightarrow 2Fe(OH)_3 + Mn^{2+} + \mathbf{2H^+}$

$2Fe(OH)_3 + \mathbf{HS^-} + \mathbf{5H^+} \rightarrow 2Fe^{2+} + S^0 + 6H_2O$

$Fe^{2+} + \mathbf{HS^-} \leftrightarrow FeS + \mathbf{H^+}$

$FeS + 2.25O_2 + 2.5H_2O \rightarrow Fe(OH)_3 + \mathbf{2H^+} + SO_4^{2-}$

$FeS_2 + 3.5O_2 + H_2O \rightarrow Fe^{2+} + 2SO_4^{2-} + \mathbf{2H^+}$

$Fe^{2+} + \mathbf{CO_3^{2-}} \leftrightarrow FeCO_3$

$NH_4^+ + 1.5O_2 \rightarrow NO_2^- + \mathbf{2H^+} + H_2O$

$0.75CH_2O + \mathbf{H^+} + NO_2^- \rightarrow 0.5N_2 + 1.25H_2O + 0.75CO_2$

$4S^0 + 3H_2O \rightarrow 2H_2S + S_2O_3^{2-} + \mathbf{2H^+}$

$2S^0 + O_2 + H_2O \rightarrow S_2O_3^{2-} + \mathbf{2H^+}$

$4S^0 + 3NO_3^- + 7H_2O \rightarrow 4SO_4^{2-} + 3NH_4^+ + \mathbf{2H^+}$

$S_2O_3^{2-} + 2O_2 + \mathbf{2OH^-} \rightarrow 2SO_4^{2-} + H_2O$

$5H_2S + 8NO_3^- + \mathbf{2OH^-} \rightarrow 5SO_4^{2-} + 4N_2 + 6H_2O$

$Ca^{2+} + \mathbf{CO_3^{2-}} \leftrightarrow CaCO_3.$

Standard alkalinity components were also affected by other reactions considered in the model (see Table 2).

Table 2. Continued.

(b)	
Name of process, reference, reaction	Parameterization in the model
	Manganese
Manganese (II) oxidation (Canfield et al., 2005) $4Mn^{2+} + O_2 + 4H^+ \rightarrow 4Mn^{3+} + 2H_2O$	$mn\_ox1 = 0.5 \times \left(1 + \tanh\left(\mathbf{Mn^{2+}} - s\_mnox\_mn2\right)\right) \times K\_mn\_ox1 \times \mathbf{Mn^{2+}} \times \frac{\mathbf{O_2}}{(\mathbf{O_2} + K\_mnox\_o2)}$
Manganese (III) oxidation (Tebo et al., 1997) $2Mn^{3+} + 3H_2O + 0.5O_2 \rightarrow 2MnO_2 + 6H^+$	$mn\_ox2 = 0.5 \times \left(1 + \tanh\left(\mathbf{Mn^{3+}} - s\_mnox\_mn2\right)\right) \times K\_mn\_ox2 \times \mathbf{Mn^{3+}} \times \frac{O_2}{(O_2 + K\_mnox\_o2)}$
Manganese (IV) reduction (Canfield et al., 2005) $2MnO_2 + 7H^+ + HS^- \rightarrow 2Mn^{3+} + 4H_2O + S^0$	$mn\_rd1 = 0.5 \times \left(1 + \tanh\left(\mathbf{Mn^{4+}} - s\_mnrd\_mn4\right)\right) \times K\_mn\_rd1 \times \mathbf{Mn^{4+}} \times \frac{\mathbf{H_2S}}{(\mathbf{H_2S} + K\_mnrd\_hs)}$
Manganese (III) reduction $2Mn^{3+} + HS^- \rightarrow 2Mn^{2+} + S^0 + H^+$	$mn\_rd2 = 0.5 \times \left(1 + \tanh\left(\mathbf{Mn^{3+}} - s\_mnrd\_mn3\right)\right) \times K\_mn\_rd2 \times \mathbf{Mn^{3+}} \times \frac{\mathbf{H_2S}}{(\mathbf{H_2S} + K\_mnrd\_hs)}$
MnS formation/dissolution (Davison, 1993): $Mn^{2+} + HS^- \leftrightarrow MnS + H^+$	$mns\_form = K\_mns\_form \times \max\left(0, \left(\frac{\mathbf{H_2S} \times \mathbf{Mn^{2+}}}{K\_mns \times \mathbf{H^+}} - 1\right)\right)$ $mns\_diss = K\_mns\_diss \times \mathbf{MnS} \times \max\left(0, \left(1 - \frac{\mathbf{H_2S} \times \mathbf{Mn^{2+}}}{K\_mns \times \mathbf{H^+}}\right)\right)$
$MnCO_3$ precipitation/dissolution (Van Cappellen and Wang, 1996): $Mn^{2+} + CO_3^{2-} \leftrightarrow MnCO_3$	$mnco3\_prec = K\_mnco3\_pres \times \max\left(0, \left(\frac{\mathbf{Mn^{2+}} \times \mathbf{CO_3}}{K\_mnco3} - 1\right)\right)$ $mnco3\_diss = K\_mnco3\_diss \times \mathbf{MnCO_3} \times \max\left(0, \left(1 - \frac{\mathbf{Mn^{2+}} \times \mathbf{CO_3}}{K\_mnco3}\right)\right)$
$MnCO_3$ oxidation by O_2 (Morgan, 2000): $2\,MnCO_3 + O_2 + 2H_2O \rightarrow 2\,MnO_2 + 2HCO_3^- + 2H^+$	$mnco3\_ox = K\_mnco3\_ox \times \mathbf{MnCO_3} \times \mathbf{O_2}$
Manganese reduction for PON (Boudreau, 1996): $(CH_2O)_{106}(NH_3)_{16}H_3PO_4 + 212MnO_2 + 318CO_2 + 106H_2O \rightarrow 424HCO_3^- + 212\,Mn^{2+} + 16NH_3 + H_3PO_4$	$DcPM\_Mn = K\_PON\_mn \times \mathbf{PON} \times \frac{\mathbf{Mn^{4+}}}{\mathbf{Mn^{4+}} + 0.5} \times (1 - 0.5 \times (1 + \tanh(\mathbf{O_2} - O2s\_dn))$
Manganese reduction for DON (Boudreau, 1996):	$DcDM\_Mn = K\_DON\_mn \times \mathbf{DON} \times \frac{\mathbf{Mn^{4+}}}{\mathbf{Mn^{4+}} + 0.5} \times (1 - 0.5 \times (1 + \tanh(\mathbf{O_2} - O2s\_dn))$
	Iron
Fe(II) oxidation with O_2 (Van Cappellen and Wang, 1996): $4Fe^{2+} + O_2 + 10H_2O \rightarrow 4Fe(OH)_3 + 8H^+$	$fe\_ox1 = 0.5 \times (1 + \tanh(\mathbf{Fe^{2+}} - s\_feox\_fe2)) \times K\_fe\_ox1 \times \mathbf{O_2} \times \mathbf{Fe^{2+}}$
Fe(II) oxidation with Mn oxide (Van Cappellen and Wang, 1996): $2Fe^{2+} + MnO_2 + 4H_2O \rightarrow 2Fe(OH)_3 + Mn^{2+} + 2\,H^+$	$fe\_ox2 = 0.5 \times \left(1 + \tanh\left(\mathbf{Fe^{2+}} - s\_feox\_fe2\right)\right) \times K\_fe\_ox2 \times \mathbf{Mn^{4+}} \times \mathbf{Fe^{2+}}$
Fe(III) reduction (Volkov, 1984): $2Fe(OH)_3 + HS^- + 5H^+ \rightarrow 2Fe^{2+} + S^0 + 6H_2O$	$fe\_rd = 0.5 \times (1.0 + \tanh(\mathbf{Fe^{3+}} - s\_feox\_fe3)) \times K\_fe\_rd \times \mathbf{Fe^{3+}} \times \frac{\mathbf{H_2S}}{\mathbf{H_2S} + K\_ferd\_hs}$
FeS formation/dissolution (Bektursunova and L'Heureux, 2011): $Fe^{2+} + HS^- \leftrightarrow FeS + H^+$	$fes\_prec = K\_fes\_form \times \max\left(0, \left(\frac{\mathbf{H_2S} \times \mathbf{Fe^{2+}}}{K\_fes \times \mathbf{H^+}} - 1\right)\right)$ $fes\_diss = K\_fes\_diss \times \mathbf{FeS} \times \max\left(0, \left(1 - \frac{\mathbf{H_2S} \times \mathbf{Fe^{2+}}}{K\_fes \times \mathbf{H^+}}\right)\right)$
FeS oxidation (Soetaert et al., 2007): $FeS + 2.25O_2 + 2.5H_2O \rightarrow Fe(OH)_3 + 2H^+ + SO_4^{2-}$	$fes\_ox = K\_fes\_ox \times \mathbf{O_2} \times \mathbf{FeS}$
Pyrite formation (Rickard and Luther, 1997; Soetaert et al., 2007): $FeS + H_2S \rightarrow FeS_2 + H_2$	$fes2\_form = K\_fes2\_form \times \mathbf{H_2S} \times \mathbf{FeS}$
Pyrite oxidation by O_2 (Wijsman et al., 2002): $FeS_2 + 3.5O_2 + H_2O \rightarrow Fe^{2+} + 2SO_4^{2-} + 2H^+$	$fes2\_ox = K\_fes2\_ox \times \mathbf{FeS_2} \times \mathbf{O_2}$
$FeCO_3$ precipitation/dissolution (Van Cappellen and Wang, 1996): $Fe^{2+} + CO_3^- \leftrightarrow FeCO_3$	$feco3\_form = K\_feco3\_form \times \max\left(0, \left(\frac{\mathbf{Fe^{2+}} \times \mathbf{CO_3}}{K\_feco3} - 1\right)\right)$ $feco3\_diss = K\_feco3\_diss \times \mathbf{FeCO_3} \times \max\left(0, \left(1 - \frac{\mathbf{Fe^{2+}} \times \mathbf{CO_3}}{K\_feco3}\right)\right)$
$FeCO_3$ oxidation by O_2 (Morgan, 2000): $2\,FeCO_3 + O_2 + 2H_2O \rightarrow 2\,FeO_2 + 2HCO_3^- + 2H^+$	$feco3\_ox = K\_feco3\_ox \times \mathbf{FeCO_3} \times \mathbf{O_2}$
Iron reduction for DON (Boudreau, 1996): $(CH_2O)_{106}(NH_3)_{16}H_3PO_4 + 424\,Fe(OH)_3 + 742CO_2 \rightarrow 848HCO_3^- + 424\,Fe^{2+} + 318\,H_2O + 16NH_3 + H_3PO_4$	$DcDM\_Fe = K\_DON\_fe \times \mathbf{DON} \times \mathbf{Fe^{3+}} \times (1.0 - 0.5 \times (1 + \tanh(\mathbf{O_2} - O2s\_dn)))$
Iron reduction for PON (Boudreau, 1996):	$DcPM\_Fe = K\_PON\_fe \times \mathbf{PON} \times \mathbf{Fe^{3+}} \times (1.0 - 0.5 \times (1 + \tanh(\mathbf{O_2} - O2s\_dn)))$

Table 2. Continued.

	Sulfur
S^0 disproportionation (Canfield et al., 2005): $4S^0+3H_2O \rightarrow 2H_2S+S_2O_3^{2-}+2H^+$	s0_disp = K_s0_disp × $\mathbf{S^0}$
Sulfide oxidation with O_2 (Volkov, 1984): $2H_2S + O_2 \rightarrow 2S^0+2H_2O$	hs_ox = K_hs_ox × $\mathbf{H_2S}$ × $\mathbf{O_2}$
S^0 oxidation with O_2 (Volkov, 1984): $2S^0+O_2+H_2O \rightarrow S_2O_3^{2-}+2H^+$	s0_ox = K_s0_ox × $\mathbf{S^0}$ × $\mathbf{O_2}$
S^0 oxidation with NO_3 (Kamyshny et al., 2013): $4S^0+3NO_3^-+7H_2O \rightarrow 4SO_4^{2-}+3NH_4^++2H^+$	s0_no3 = K_s0_no3 × $\mathbf{NO_3}$ × $\mathbf{S^0}$
S_2O_3 oxidation with O_2 (Volkov, 1984): $S_2O_3^{2-}+2O_2+2OH^- \rightarrow 2SO_4^{2-}+H_2O$	s2o3_ox = K_s2o3_ox × $\mathbf{S_2O_3}$ × $\mathbf{O_2}$
S_2O_3 oxidation with NO_3 (Kamyshny et al., 2013): $S_2O_3^{2-}+NO_3^-+2H_2O \rightarrow 2SO_4^{2-}+NH_4^+$	s2o3_no3 = K_s2o3_no3 × $\mathbf{NO_3}$ × $\mathbf{S_2O_3}$
Thiodenitrification (Schippers and Jorgensen, 2002; Volkov, 1984): $5H_2S+8NO_3^-+2OH^- \rightarrow 5SO_4^{2-}+4N_2+6H_2O$	hs_no3 = K_hs_no3 × $\mathbf{H_2S}$ × $\mathbf{NO_3}$
POM sulfate reduction 1st and 2nd stages (Boudreau, 1996): $(CH_2O)_{106}(NH_3)_{16}H_3PO_4+53SO_4^{2-} \rightarrow 106HCO_3^-+16NH_3+H_3PO_4+53H_2S$	so4_rd_PM = K_so4_rd × F_sox × F_snx × $\mathbf{SO_4}$ × **PON** s2o3_rd_PM = K_s2o3_rd × F_sox × F_snx × $\mathbf{S_2O_3}$ × **PON** F_sox = 1 − 0.5 × (1.0 + tanh($\mathbf{O_2}$ − s_omso_o2)) F_snx = 1 − 0.5 × (1.0 + tanh($\mathbf{NO_3}$ − s_omso_no3)) DcPM_SO4 = $\frac{16}{53}$ × (so4_rd_PM + s2o3_rd_PM)
DOM sulfate reduction 1st and 2nd stages (Boudreau, 1996):	so4_rd_DM = K_so4_rd × F_sox × F_snx × $\mathbf{SO_4}$ × **DON** s2o3_rd_DM = K_s2o3_rd × F_sox × F_snx × $\mathbf{S_2O_3}$ × **DON** DcDM_SO4 = $\frac{16}{53}$ × (so4_rd_PM + s2o3_rd_PM)
(c)	
Name of process, reference, reaction	Parameterization in the model
	Carbon and Alkalinity
$CaCO_3$ formation/dissolution (Luff et al., 2001): $Ca^{2+}+CO_3^2 \leftrightarrow CaCO_3$	caco3_form = K_caco3_form × max(0, $\left(\frac{\mathbf{Ca^{2+}}\times\mathbf{CO_3}}{\text{K\_caco3}}-1\right)$) caco3_diss = K_caco3_diss × $\mathbf{CaCO_3}$ × max(0, $\left(1-\frac{\mathbf{Ca^{2+}}\times\mathbf{CO_3}}{\text{K\_caco3}}\right)^{4.5}$
CH_4 formation from PON, methanogenesis (Boudreau, 1996): $(CH_2O)_{106}(NH_3)_{16}H_3PO_4 \rightarrow 53CO_2+53CH_4+16NH_3+H_3PO_4$	DcPM_CH4 = K_PON_ch4 × F_sox × F_snx × F_ssx × **PON** F_sox = 1 − 0.5 × (1.0 + tanh($\mathbf{O_2}$ − s_omso_o2)) F_snx = 1 − 0.5 × (1.0 + tanh($\mathbf{NO_3}$ − s_omso_no3)) F_ssx = 1 − 0.5 × (1.0 + tanh($\mathbf{SO_4}$ − s_omch_so4))
CH_4 formation from DON, methanogenesis (Boudreau, 1996)	DcDM_CH4 = K_DON_ch4 × F_sox × F_snx × F_ssx × **DON**
CH_4 oxidation by O_2 (Boudreau, 1996): $CH_4+2O_2 \rightarrow CO_2+2H_2O$	ch4_o2 = K_ch4_o2 × $\mathbf{CH_4}$ × $\mathbf{O_2}$
Alkalinity changes (Dickson, 1992; Wolf-Gladrow et al., 2007)	dAlk = −Nitrif1 + Denitr2_PM + Denitr2_DM + 2 × ($so4_{rd}$ + $s2o3_{rd}$) + mn_ox1 − 3 × mn_ox2 + 3 × mn_rd1 − mn_rd2 − 2 × mns_form + 2 × mns_diss − 2 × mnco3_form + 2 × mnco3_diss + 26.5 × ($DcDM_{Mn}$ + $DcPM_{Mn}$) − 2 × fe_ox1 − fe_ox2 + 2 × fe_rd − fes_form + fes_diss − 2 × fes_ox − 2 × fes2_ox + 53 × ($DcDM_{Fe}$ + $DcPM_{Fe}$) − 0.5 × Disprop + s0_ox − 0.5 × s_no3 − s2o3_ox − 0.4 × hs_no3 − 2 × caco3_form + 2 × caco3_diss + GrowthPhy × $\left(\frac{\text{LimNO3}}{\text{LimN}}\right)$ − GrowthPhy × $\left(\frac{\text{LimNH4}}{\text{LimN}}\right)$

2.1.4 Carbonate system

Equilibration of the carbonate system was considered as a fast process occurring within seconds (Zeebe and Wolf-Gladrow, 2001). Accordingly, the equilibrium solution was calculated at every time step using an iterative procedure. The carbonate system was described using standard approaches (Lewis and Wallace, 1998; Munhoven, 2013; Roy et al., 1993; Wanninkhof, 2014; Wolf-Gladrow et al., 2007; Zeebe and Wolf-Gladrow, 2001). The set of constants of Roy et al. (1993) was used for carbonic acid. Constants for boric, hydrofluoric, and hydrogen sulfate alkalinity were calculated according to Dickson (1992), for silicic alkalinity according to Millero (1995), for ammonia alkalinity according to Luff et al. (2001), and for hydrogen sulfide alkalinity according to Luff et al. (2001) and Volkov (1984). The ion product of

Table 2. Continued.

(d)	
Name of process, reference, reaction	Parameterization in the model
	Phytoplankton
Influence of the irradiance on photosynthesis	$\mathrm{LimLight} = (\mathrm{Iz} / \mathrm{Iopt}) \times \mathrm{e}^{(1-\mathrm{Iz}/\mathrm{Iopt})}$
Influence of temperature on photosynthesis	$\mathrm{LimT} = \mathrm{e}^{(\mathrm{bm}\times\mathrm{t}-\mathrm{cm})}$
Dependence of photosynthesis on P	$\mathrm{LimP} = \frac{(\mathbf{PO_4}/\mathbf{Phy})^2}{(\mathrm{K\_po4\_lim}\times\mathrm{r\_n\_p})^2+(\mathbf{PO_4}/\mathbf{Phy})^2}$
Dependence of photosynthesis on NO_3	$\mathrm{LimNO_3} = \frac{((\mathbf{NO_3}+\mathbf{NO_2})/\mathbf{Phy})^2}{\mathrm{K\_nox\_lim}^2+((\mathbf{NO_3}+\mathbf{NO_2})/\mathbf{Phy})^2}\exp(-\mathrm{K\_\_psi}\frac{(\mathbf{NH_4}/\mathbf{Phy})^2}{\mathrm{K\_nh4\_lim}^2+(\mathbf{NH_4}/\mathbf{Phy})^2})$
Dependence of photosynthesis on NH_4	$\mathrm{LimNH_4} = \frac{\left(\frac{\mathbf{NH_4}}{\mathbf{Phy}}\right)^2}{\mathrm{K\_nh4\_lim}^2+\left(\frac{\mathbf{NH_4}}{\mathbf{Phy}}\right)^2}(1-\exp(-\mathrm{K\_\_psi}\frac{(\mathbf{NH_4}/\mathbf{Phy})^2}{\mathrm{K\_nh4\_lim}^2+(\mathbf{NH_4}/\mathbf{Phy})^2}))$
Influence of N on photosynthesis	$\mathrm{LimN} = \mathrm{LimNO_3} + \mathrm{LimNH_4}$
Growth of phytoplankton	$\mathrm{GrowthPhy} = \mathrm{K\_phy\_gro} \times \mathrm{LimLight} \times \mathrm{LimT} \times \min(\mathrm{LimP}, \mathrm{LimN}) \times \mathbf{Phy}$
Excretion rate of phytoplankton	$\mathrm{ExcrPhy} = \mathrm{K\_phy\_exc} \times \mathbf{Phy}$
Phytoplankton mortality rate	$\mathrm{MortPhy} = (\mathrm{K\_phy\_mrt} + 0.45 \times (0.5 - 0.5 \times \tanh(\mathbf{O_2} - 60)) + 0.45 \times (0.5 - 0.5 \times \tanh(\mathbf{O_2} - 20))) \times \mathbf{Phy}$
	Heterotrophs
Grazing of heterotrophs	$\mathrm{Grazing} = \mathrm{GrazPhy} + \mathrm{GrazPOP} + \mathrm{GrazBact}$
Grazing of Het on phytoplankton	$\mathrm{GrazPhy} = \mathrm{K\_het\_phy\_gro} \times \mathbf{Het} \times \frac{(\mathbf{Phy}/(\mathbf{Het}+10^{-4}))^2}{\mathrm{K\_het\_phy\_lim}^2+(\mathbf{Phy}/(\mathbf{Het}+10^{-4}))^2}$
Grazing of Het on detritus	$\mathrm{GrazPOP} = \mathrm{K\_het\_pom\_gro} \times \mathbf{Het} \times \frac{(\frac{\mathbf{PON}}{\mathbf{Het}+10^{-4}})^2}{\mathrm{K\_het\_pom\_lim}^2+(\frac{\mathbf{PON}}{\mathbf{Het}+10^{-4}})^2}$
Grazing of Het on bacteria	$\mathrm{GrazBact} = \mathrm{GrazBaae} + \mathrm{GrazBaan} + \mathrm{GrazBhae} + \mathrm{GrazBhan}$
Grazing of Het on bacteria autotrophic aerobic	$\mathrm{GrazBaae} = \mathrm{K\_het\_pom\_gro} \times \mathbf{Het} \times \frac{(\mathbf{Baae}/(\mathbf{Het}+10^{-4}))^2}{\mathrm{limGrazBac}^2+(\mathbf{Baae}/(\mathbf{Het}+10^{-4}))^2}$
Grazing of Het on bacteria autotrophic anaerobic	$\mathrm{GrazBaan} = 0.5 \times \mathrm{K\_het\_pom\_gro} \times \mathbf{Het} \times \frac{(\mathbf{Baan}/(\mathbf{Het}+10^{-4}))^2}{\mathrm{limGrazBac}^2+(\mathbf{Baan}/(\mathbf{Het}+10^{-4}))^2}$
Grazing of Het on bacteria heterotrophic aerobic	$\mathrm{GrazBhae} = \mathrm{K\_het\_pom\_gro} \times \mathbf{Het} \times \frac{(\mathbf{Bhae}/(\mathbf{Het}+10^{-4}))^2}{\mathrm{limGrazBac}^2+(\mathbf{Bhae}/(\mathbf{Het}+10^{-4})^2}$
Grazing of Het on bacteria heterotrophic anaerobic	$\mathrm{GrazBhan} = 1.3 \times \mathrm{K\_het\_pom\_gro} \times \mathbf{Het} \times \frac{(\mathbf{Bhan}/\mathbf{Het}+0.0001)^2}{\mathrm{limGrazBac}^2+(\mathbf{Bhan}/\mathbf{Het}+10^{-4})^2}$
Respiration rate of Het	$\mathrm{RespHet} = \mathrm{K\_het\_res} \times \mathbf{Het} \times (0.5 + 0.5 \times \tanh(\mathbf{O_2} - 20))$
Mortality of Het	$\mathrm{MortHet} = \mathbf{Het} \times \left(\begin{array}{l} 0.25 + 0.3 \times (0.5 - 0.5 \times \tanh(\mathbf{O_2} - 20)) \\ + 0.45 \times (0.5 + 0.4 \times \tanh(\mathbf{H_2S} - 10)) \end{array}\right)$
	Bacteria
Growth rate of bacteria aerobic autotrophic	$(\mathrm{ChemBaae} = \mathrm{Nitrif1} + \mathrm{Nitrif2} + \mathrm{mn\_ox1} + \mathrm{fe\_ox1} + \mathrm{s2o3\_ox} + \mathrm{s0\_ox} + \mathrm{anammox}) \times \mathrm{k_{Baae_{gro}}} \times \mathbf{Baae} \times \min(\frac{(\mathbf{NH_4}/((\mathbf{Baae}+10^{-4})^2}{\mathrm{limBaae}^2+(\mathbf{NH_4}/(\mathbf{Baae}+10^{-4}))^2}, \frac{(\mathbf{PO_4}/(\mathbf{Baae}+10^{-4}))^2}{\mathrm{limBaae}^2+(\mathbf{PO_4}/(\mathbf{Baae}+10^{-4}))^2})$
Rate of mortality of bacteria aerobic autotrophic	$\mathrm{MortBaae} = \mathrm{K\_Baae\_mrt} + \mathrm{K\_Baae\_mrt\_h2s} \times 0.5 \times (1 - \tanh(1 - \mathbf{H_2S})) \times \mathbf{Baae}^2$
Growth rate of bacteria aerobic heterotrophic	$\mathrm{HetBhae} = (\mathrm{DcPM\_O2} + \mathrm{DcDM\_O2}) \times \mathrm{K\_Bhae\_gro} \times \mathbf{Bhae} \times \frac{(\mathbf{DON}/(\mathbf{Bhae}+10^{-4}))^2}{\mathrm{limBhae}^2+(\mathbf{DON}/(\mathbf{Bhae}+10^{-4}))^2}$
Rate of mortality of bacteria aerobic heterotrophic	$\mathrm{MortBhae} = \mathrm{K\_Bhae\_mrt} + \mathrm{K\_Bhae\_mrt\_h2s} \times \mathbf{Bhae} \times 0.5 \times (1 - \tanh(1 - \mathbf{H_2S}))$
Growth rate of bacteria anaerobic autotrophic	$\mathrm{ChemBaan} = (\mathrm{mn\_rd1} + \mathrm{mn\_rd2} + \mathrm{fe\_rd} + \mathrm{hs\_ox} + \mathrm{hs\_no3}) \times \mathrm{K\_Baan\_gro} \times \mathbf{Baan} \times \min?(\frac{(\mathbf{NH4}/(\mathbf{Baan}+10^{-4}))^2}{\mathrm{limBaan}^2+(\mathbf{NH4}/(\mathbf{Baan}+10^{-4}))^2}$
Rate of mortality of bacteria anaerobic autotrophic	$\mathrm{MortBaan} = \mathrm{K\_Baan\_mrt} \times \mathbf{Baan}$
Growth rate of bacteria anaerobic heterotrophic	$\mathrm{HetBhan} = (\mathrm{DcPM\_NOX} + \mathrm{DcDM\_NOX} + \mathrm{DcDM\_Mn} + \mathrm{DcPM\_Mn} + \mathrm{DcDM\_Fe} + \mathrm{DcPM\_Fe} + \mathrm{DcDM\_SO4} + \mathrm{DcPMSO4} + \mathrm{DcDM\_CH4} + \mathrm{DcPM\_CH4}) \times \mathrm{K\_Bhan\_gro} \times \mathbf{Bhan} \times \frac{(\mathbf{DON}/(\mathbf{Bhan}+10^{-4}))^2}{\mathrm{limBhan}^2+(\mathbf{DON}/(\mathbf{Bhan}+10^{-4}))^2}$
Rate of mortality of bacteria anaerobic heterotrophic	$\mathrm{MortBhan} = \mathrm{K\_Bhan\_mrt} + \mathrm{K\_Bhan\_mrt\_o2} \times \mathbf{Bhan} \times (0.5 + 0.5 \times \tanh(1 - \mathbf{O_2}))$
Summarized OM mineralization	$\mathrm{Dc\_OM\_total} = \mathrm{DcDM\_O2} + \mathrm{DcPM\_O2} + \mathrm{DcPM\_NOX} + \mathrm{DcDM\_NOX} + \mathrm{DcDM\_Mn} + \mathrm{DcPM\_Mn} + \mathrm{DcDM\_Fe} + \mathrm{DcPM\_Fe} + \mathrm{DcDM\_SO4} + \mathrm{DcPM\_SO4} + 0.5 \times (\mathrm{DcDM\_CH4} + \mathrm{DcPM\_CH4})$

water was calculated according to Millero (1995). Total scale pH was calculated using the Newton–Raphson method with the modifications proposed in Munhoven (2013). Precipitation and dissolution of calcium carbonate were modeled following the approach of Luff et al. (2001) (Table 2).

2.1.5 Physical environment

BROM-biogeochemistry can be coupled online with various hydrodynamic models using FABM, but this may require extensive adaptation of the hydrodynamic model to resolve the BBL and upper sediments. We have therefore developed a simple 1-D offline transport-reaction model, BROM-transport, whose model domain spans the water column, BBL, and upper layers of the sediments, with enhanced spatial resolution in the BBL and sediments. All options and parameter values for BROM-transport are specified in a runtime input file brom.yaml. A step-by-step guide to running BROM-transport is provided in Appendix A.

2.1.6 BROM-transport model formulation

The time–space evolution of state variables in BROM-transport is described by a system of 1-D transport-reaction equations in Cartesian coordinates. In the water column, the dynamics are

$$\frac{\partial \hat{C}_i}{\partial t} = \frac{\partial}{\partial z} D \frac{\partial \hat{C}_i}{\partial z} - \frac{\partial}{\partial z} v_i \hat{C}_i + \varepsilon_\mathrm{h} \left(\hat{C}_{0i} - \hat{C}_i \right) + T_{\mathrm{birr}(i)} + R_i, \quad (1)$$

where $\hat{C}_i$ is the concentration in units [mmol m^{-3} total volume] of the ith state variable, $D(z,t)$ is the vertical diffusivity, v_i is the settling or sinking velocity, $\varepsilon_\mathrm{h}(z,t)$ is a rate of horizontal mixing with an external concentration $\hat{C}_{0i}(z,t)$ (or alternatively, a restoring rate to a climatological concentration), $T_{\mathrm{birr}(i)}$ is a tendency due to bioirrigation (only non-zero for dissolved substances in the bottom layer of the water column; see below), and R_i is the combined sources minus sinks (in this study provided by BROM-biogeochemistry, but in principle any biogeochemical model in FABM could be used). Values for D, ε_h, $\hat{C}_{0i}$, and other forcings used by R_i are configured at runtime through input files (see Sect. 2.2.7). Sinking velocities v_i are non-zero only for particulate (non-dissolved) variables and are determined at each time step by the biogeochemical module (through FABM). BROM-biogeochemistry assumes constant sinking velocities for phytoplankton, zooplankton, bacteria, detritus, and inorganic particles (Table 3e).

In the sediments, dissolved substances or solutes obey the dynamics

$$\varphi \frac{\partial C_i}{\partial t} = \frac{\partial}{\partial z} \varphi D_C \frac{\partial C_i}{\partial z} - \frac{\partial}{\partial z} \varphi u C_i + T_{\mathrm{birr}C(i)} + R_i, \quad (2)$$

where φ is the porosity (assumed constant in time), D_C is the total solute diffusivity, u is the solute burial velocity, and C_i is the porewater concentration in units [mmol m^{-3} porewater]. Particulate substances become part of the solid matrix in the sediments. These obey

$$(1-\varphi) \frac{\partial B_i}{\partial t} = \frac{\partial}{\partial z} (1-\varphi) D_\mathrm{B} \frac{\partial B_i}{\partial z} - \frac{\partial}{\partial z} (1-\varphi) w B_i + R_i, \quad (3)$$

where D_B is the particulate (bioturbation) diffusivity, w is the particulate burial velocity, and B_i is the particulate concentration in units [mmol m^{-3} total solids].

The porosity $\varphi(z)$ in Eqs. (2) and (3) is prescribed as an exponential decay, following Soetaert et al. (1996):

$$\varphi = \varphi_\infty + (\varphi_0 - \varphi_\infty) e^{\frac{-(z-z_\mathrm{SWI})}{\delta}}, \quad (4)$$

where φ_∞ is the deep (compacted) porosity, φ_0 is the sediment surface porosity, z_SWI is the depth of the SWI, and δ is a decay scale defining the rate of compaction.

Diffusion within the sediments is assumed to be strictly "intraphase" (Boudreau, 1997), hence the Fickian gradients in Eqs. (2) and (3) are formed using the concentration per unit volume porewater for solutes and per unit volume total solids for particulates. The total solute diffusivity $D_C = D_\mathrm{m} + D_\mathrm{B}$, where D_m is the apparent molecular/ionic diffusivity and D_B is the bioturbation diffusivity due to animal movement and ingestion/excretion. The apparent molecular diffusivity $D_\mathrm{m}(z) = \theta^{-2} D_0 \frac{\mu_0}{\mu_\mathrm{sw}}$ is derived from the infinite-dilution molecular diffusivity D_0 (an input parameter) assuming a constant relative dynamic viscosity $\frac{\mu_0}{\mu_\mathrm{sw}}$ (default value 0.94, cf. Boudreau, 1997, Table 4.10) and a tortuosity parameterized as $\theta^2 = 1 - 2\ln\varphi$ from Boudreau (1997, Eq. 4.120). The bioturbation diffusivity $D_\mathrm{B}(z,t)$ is modeled as a Michaelis–Menten function of the dissolved oxygen concentration in the bottom layer of the water column:

$$D_\mathrm{B}(z,t) = D_{\mathrm{Bmax}}(z) \frac{\mathrm{O_{2s}}}{\mathrm{O_{2s}} + K_{\mathrm{O2s}}}, \quad (5)$$

where $D_{\mathrm{Bmax}}(z)$ is a constant over a fixed mixed layer depth in the surface sediments, then decays to zero with increasing depth, and K_{O2s} is a half-saturation constant. The rationale for Eq. (5) is that the benthic animals that cause bioturbation require a source of oxygen at the sediment surface for respiration.

Diffusion between the sediments and water column, i.e., across the SWI, raises a subtle issue in regard to particulates. Here, any diffusive flux cannot be strictly intraphase, because particulates are modeled as [mmol m^{-3} total solids] in the sediments but as [mmol m^{-3} total volume] in the water column. In BROM-transport, the bottom layer of the water column is considered a "fluff layer"; particles enter through the upper interface at their sinking velocity and leave through the SWI at the particulate burial velocity. It follows that a portion of the particulate matter in the fluff layer must be considered as settled fluff, but that portion is not predicted by the

Table 3. Parameter names, notations, values, and units of the coefficients used in the model: **(a)** nutrients and oxygen; **(b)** redox metals and sulfur; **(c)** carbon; **(d)** ecosystem parameters; **(e)** sinking.

(a)				
Parameter	Notation	Units	Value	Reference ranges
		Nitrogen		
Specific rate of DON oxidation with O_2	K_DON_ ox	d^{-1}	1×10^{-2}	0.1 (Savchuk, 2002)
Specific rate of PON oxidation with O_2	K_PON_ ox	d^{-1}	2×10^{-3}	0.002 (Savchuk, 2002)
Temperature control threshold coefficient for OM decay	Tda	°C	13	13 (Burchard et al., 2006)
Temperature control coefficient for OM decay	beta_da	–	20	20 (Burchard et al., 2006)
Half-saturation constant of O_2 for OM mineralization	K_omox_o2	µM	1	1 (Yakushev, 2013)
Specific rate of autolysis, PON to DON	K_PON_DON	d^{-1}	0.1	0.02 (Burchard et al., 2006)
Half-saturation constant for uptake of NO_3+NO_2	K_nox_lim	µM	0.12	0.5 (Gregoire and Lacroix, 2001)
Half-saturation constant for uptake of NH_4	K_nh4_ lim	µM	2×10^{-2}	0.2 (Gregoire and Lacroix, 2001)
Strength of NH_4 inhibition of NO_3 uptake constant	K_psi	–	1.46	1.46 (Gregoire and Lacroix, 2001)
Specific rate of the 1st stage of nitrification	K_nitrif1	d^{-1}	1×10^{-2}	0.01 (Yakushev, 2013)
Specific rate of the 2nd stage of nitrification	K_nitrif2	d^{-1}	0.1	0.1 (Yakushev, 2013)
Specific rate of 1st stage of denitrification	K_denitr1	d^{-1}	0.16	0.16 (Yakushev and Neretin, 1997), 0.5 (Savchuk, 2002)
Specific rate of 2nd stage of denitrification	K_denitr2	d^{-1}	0.25	0.22 (Yakushev and Neretin, 1997)
Half-saturation of NO_3 for OM denitrification	k_omno_no3	µM N	1×10^{-3}	1×10^{-3} (Yakushev, 2013)
Half-saturation of NO_2 for OM denitrification	k_omno_no2	µM N	1×10^{-3}	1×10^{-3} (Yakushev, 2013)
Specific rate of thiodenitrification	K_hs_no3	$\mu M^{-1}\ d^{-1}$	0.8	0.8 (Yakushev and Neretin, 1997), 0.015 (Gregoire and Lacroix, 2001)
Specific rate of anammox	K_anammox	d^{-1}	0.8	0.8 (Gregoire and Lacroix, 2001), 0.03 (Yakushev et al., 2007)
		Oxygen		
Half-saturation constant for nitrification	O2s_nf	µM	5.0	10 (Gregoire and Lacroix, 2001)
Half-saturation constant for denitrification anammox, Mn reduction	O2s_dn	µM	10	40 (Savchuk, 2002)
Threshold value of O_2 for OM mineralization	s_omox_o2	µM	1×10^{-2}	1×10^{-2} (Yakushev, 2013)
Threshold value of O_2 for OM denitrification	s_omno_o2	µM	25	25 (Yakushev, 2013)
Threshold value of O_2 for OM sulfate reduction	s_omso_o2	µM	25	25 (Yakushev, 2013)
Threshold value of NO for OM sulfate reduction	s_omso_ no3	µM	5	5 (Yakushev, 2013)
		Stoichiometric coefficients		
N / P	r_n_p	–	16	Richards (1965)
O / N	r_o_n	–	6.625	Richards (1965)
C / N	r_c_n	–	8	Richards (1965)
Si / N	r_si_n	–	1	Richards (1965)
Fe / N	r_fe_n	–	26.5	Boudreau (1996)
Mn / N	r_mn_n	–	13.25	Boudreau (1996)
		Phosphorus		
Half-saturation constant for uptake of PO_4 by phytoplankton	K_po4_lim	µM	0.02	0.01 (Yakushev et al., 2007)
Fe / P ratio in complexes with Fe oxides	r_fe_p	–	2.7	(Yakushev et al., 2007)
Mn / P ratio in complexes with Mn(III)	r_mn_p	–	0.67	(Yakushev et al., 2007)
		Silicon		
Specific rate of Si dissolution	K_sipart_diss	d^{-1}	0.008	0.008 (Popova and Srokosz, 2009)
Half-saturation constant for uptake of Si by phytoplankton	K_si_lim	–	0.1	0.1 (Popova and Srokosz, 2009)
Fe / P ratio in complexes with Fe oxides	r_fe_si	–	2.7	2.7 (Yakushev et al., 2007)

model. BROM-transport therefore offers two approaches. In the first approach, the bioturbation diffusivity is set to zero on the SWI, so that only solutes can diffuse across the SWI by molecular diffusion. Since the present version of BROM-transport does not parameterize resuspension through the SWI due to fluid turbulence, the SWI thus becomes a one-way street for particulate matter, whose components can only reenter the water column after dissolution. In the second approach, the bioturbation diffusivity is given by Eq. (5) on the SWI, but the bioturbation flux is interphase, mixing concentrations in units [mmol m^{-3} total volume] for both solutes and particulates. This approach is appropriate if bioturbation can be assumed to exchange fluff and sediment, or if it contributes significantly to particulate resuspension.

The burial velocities u and w in Eqs. (2) and (3) can be inferred from the porosity profile under the assumptions of steady-state compaction (φ constant in time) and no externally impressed porewater flow (Berner, 1971, 1980; Boudreau, 1997; Meysman et al., 2005). Here, BROM-transport again offers two approaches. In the first approach,

Table 3. Continued.

(b)

Parameter	Notation	Units	Value	Reference ranges
Manganese				
Specific rate of Mn(II) oxidation to Mn(III) with O_2	K_mn_ox1	d^{-1}	0.1	0.18–1.9 $M yr^{-1}$; (Tebo, 1991) 2 d^{-1}; (Yakushev et al., 2007)
Specific rate of Mn(IV) reduction to Mn(III) with H_2S	K_mn_rd1	d^{-1}	0.5	22 d^{-1}; (Yakushev et al., 2007)
Specific rate of Mn(III) oxidation to Mn(IV) with O_2	K_mn_ox2	d^{-1}	0.2	18 d^{-1}; (Yakushev et al., 2008)
Specific rate of Mn(III) reduction to Mn(II) with H_2S	K_mn_rd2	d^{-1}	1	0.96–3.6 $M yr^{-1}$; (Tebo, 1991) 2 d^{-1}; (Yakushev et al., 2007)
Specific rate of formation of MnS from Mn(II) and H_2S	K_mns_form	d^{-1}	1×10^{-5}	Assumed
Specific rate of dissolution of MnS to Mn(II) and H_2S	K_mns_diss	d^{-1}	5×10^{-4}	Assumed
Solubility product for MnS	K_mns	M	1500	7.4×10^{-18} M (Brezonik and Arnold, 2011)
Solubility product for $MnCO_3$	K_mnco3	M	1	3.4×10^{-10}–10^{-13} M (Jensen et al., 2002)
Specific rate of $MnCO_3$formation	K_mnco3_ form	d^{-1}	3×10^{-4}	10^{-4}–10^{-2} mol g^{-1} yr^{-1}; (Wersin, 1990; Wollast, 1990)
Specific rate of $MnCO_3$ dissolution	K_mnco3_ diss	d^{-1}	7×10^{-4}	10^{-2}–10^{3} yr^{-1}; (Wersin, 1990; Wollast, 1990)
Specific rate of MnCO3 oxidation	K_mnco3_ox	d^{-1}	27×10^{-4}	Assumed
Specific rate of DON Oxidation with Mn(IV)	K_DON_Mn	d^{-1}	1×10^{-3}	1×10^{-3} (Yakushev et al., 2007)
Specific rate of PON Oxidation with Mn(IV)	K_PON_Mn	d^{-1}	1×10^{-3}	1×10^{-3} (Yakushev et al., 2007)
Threshold value of Mn(II) oxidation	s_mnox_mn2	µM Mn	1×10^{-2}	1×10^{-2} (Yakushev et al., 2007)
Threshold value of Mn(III) oxidation	s_mnox_mn3	µM Mn	1×10^{-2}	1×10^{-2} (Yakushev et al., 2007)
Threshold value of Mn(IV) reduction	s_mnrd_mn4	µM Mn	1×10^{-2}	1×10^{-2} (Yakushev et al., 2007)
Threshold value of Mn(III) reduction	s_mnrd_mn3	µM Mn	1×10^{-2}	1×10^{-2} (Yakushev et al., 2007)
Half-saturation constant of Mn oxidation	K_mnox_o2	µM O_2	2	2 (Yakushev et al., 2007)
Iron				
Specific rate of Fe(II) to Fe(III) oxidation with O_2	K_fe_ox1	d^{-1}	0.5	2×10^{9} M yr^{-1}; (Boudreau, 1996); 4 d^{-1}; (Yakushev et al., 2007)
Specific rate of Fe(II) to Fe(III) oxidation with MnO_2	K_fe_ox2	d^{-1}	1×10^{-3}	10^{4}–10^{8} M yr^{-1}; (Boudreau, 1996); 1 d^{-1}; (Yakushev et al., 2007)
Specific rate of Fe(III) to Fe(II) reduction with H_2S	K_fe_rd	d^{-1}	0.5	1×10^{4} M yr^{-1}; (Boudreau, 1996); 0.05 d^{-1}; (Yakushev et al., 2007)
Solubility product for FeS	K_fes	µM	2510	2.51×10^{-6} mol cm^{-3} (Bektursunova and L'Heureux, 2011)
Specific rate of FeS formation from Fe(II) and H_2S	K_fes_form	d^{-1}	5×10^{-4}	5×10^{-6}–10^{-3} M yr^{-1}; (Boudreau, 1996; Hunter et al., 1998; Bektursunova and L'Heureux, 2011)
Specific rate of FeS dissolution to Fe(II) and H_2S	K_fes_diss	d^{-1}	1×10^{-6}	1×10^{-3} yr^{-1} (Hunter et al., 1998; Bektursunova and L'Heureux, 2011)
Specific rate of FeS oxidation with O_2	K_fes_ox	d^{-1}	1×10^{-3}	2×10^{7}–3×10^{5} M yr^{-1}; (Boudreau, 1996; Van Cappellen and Wang, 1996)
Specific rate of DON oxidation with Fe(III)	K_DON_ fe	d^{-1}	5×10^{-5}	5×10^{-5} (Yakushev et al., 2007)
Specific rate of PON oxidation with Fe(III)	K_PON_ fe	d^{-1}	1×10^{-5}	1×10^{-5} (Yakushev et al., 2007)
Specific rate of FeS_2 formation by reaction of FeS with H_2S	K_fes2_form	d^{-1}	1×10^{-6}	8.9×10^{-6} M day^{-1}; (Rickard and Luther, 1997)
Specific rate of FeS_2 oxidation with O_2	K_fes2_ox	d^{-1}	4.4×10^{-4}	(Bektursunova and L'Heureux, 2011)
Threshold value of Fe(II) reduction	s_feox_fe2	µM Fe	1×10^{-3}	1×10^{-3} (Yakushev et al., 2007)
Threshold value of Fe(III) reduction	s_ferd_fe3	µM Fe	1×10^{-2}	1×10^{-2} (Yakushev et al., 2007)
Solubility product for $FeCO_3$	K_feco3	µM	15	3.8×10^{-11}–6.4×10^{-12} M (Jensen et al., 2002)
Specific rate of $FeCO_3$ dissolution	K_feco3_ diss	d^{-1}	7×10^{-4}	2.5×10^{-1}–10^{-2} yr^{-1}; (Wersin, 1990; Wollast, 1990)
Specific rate of $FeCO_3$ formation	K_feco3_form	d^{-1}	3.4×10^{-4}	10^{-6}–10^{-2} mol/g yr; (Boudreau, 1996; Wersin, 1990; Wollast, 1990)
Specific rate of $FeCO_3$ oxidation with O_2	K_feco3_ox	d^{-1}	2.7×10^{-3}	Assumed
Sulfur				
Specific rate of H_2S oxidation to S^0 with O_2	K_hs_ox	d^{-1}	0.5	0.5 (Yakushev et al., 2007)
Specific rate of S^0 oxidation with O_2	K_s0_ox	d^{-1}	2×10^{-2}	2×10^{-2} (Yakushev et al., 2007)
Specific rate of S^0 oxidation with NO_3	K_s0_no3	d^{-1}	0.9	0.9 (Yakushev et al., 2007)
Specific rate of S_2O_3 oxidation with O_2	K_s2o3_ox	d^{-1}	1×10^{-2}	1×10^{-2} (Yakushev et al., 2007)
Specific rate of S_2O_3 oxidation with NO_3	K_s2o3_no3	d^{-1}	1×10^{-2}	1×10^{-2} (Yakushev et al., 2007)
Specific rate of OM reduction with sulfate	K_so4_rd	d^{-1}	5×10^{-6}	5×10^{-6} (Yakushev et al., 2007)
Specific rate of OM reduction with thiosulfate	K_s2o3_rd	d^{-1}	1×10^{-3}	1×10^{-3} (Yakushev et al., 2007)
Specific rate of S^0 disproportionation	K_s0_ disp	d^{-1}	1×10^{-3}	1×10^{-3} (Yakushev et al., 2007)
Half-saturation of Mn reduction	K_mnrd_hs	µM S	1	1 (Yakushev et al., 2007)
Half-saturation of Fe reduction	K_ferd_hs	µM S	1	1 (Yakushev et al., 2007)

Table 3. Continued.

(c)

Parameter	Notation	Units	Value	Reference ranges
Specific rate of $CaCO_3$ dissolution	K_caco3_ diss	d^{-1}	3	Wide ranges are given in Luff et al. (2001)
Specific rate of $CaCO_3$ formation	K_caco3_prec	d^{-1}	2×10^{-4}	Wide ranges are given in Luff et al. (2001)
Solubility product constant for $CaCO_3$	K_caco3			Calculated as a function of T, S (Roy et al., 1993)
Specific rate of CH_4 formation from DON	K_DON_ ch4	d^{-1}	5×10^{-5}	Lopes et al. (2011)
Specific rate of CH_4 formation from PON	K_PON_ ch4	d^{-1}	1×10^{-5}	Lopes et al. (2011)
Specific rate of CH_4 oxidation with O_2	K_ch4_o2	$uM^{-1}d^{-1}$	0.14	0.14 (Lopes et al., 2011)
Specific rate of CH_4 oxidation with SO_4	K_ch4_so4	$uM^{-1}d^{-1}$	0.0000274	0.0274 m^3/mol^{-1} day^{-1} (Lopes et al., 2011)

(d)

Parameter	Notation	Units	Value	Reference ranges
Bacteria				
Baae maximum specific growth rate	K_Baae_gro	d^{-1}	2×10^{-2}	2×10^{-2} (Yakushev et al., 2007)
Baae specific rate of mortality	K_Baae_mrt	d^{-1}	5×10^{-3}	5×10^{-3} (Yakushev et al., 2007)
Baae increased specific rate of mortality due to H_2S	K_Baae_mrt_h2s	d^{-1}	0.899	0.899 (Yakushev et al., 2007)
Bhae maximum specific growth rate	K_Bhae_gro	d^{-1}	0.5	0.5 (Yakushev et al., 2007)
Bhae specific rate of mortality	K_Bhae_mrt	d^{-1}	2×10^{-2}	2×10^{-2} (Yakushev et al., 2007)
Bhae increased specific rate of mortality due to H_2S	K_Bhae_mrt_h2s	d^{-1}	0.799	0.799 (Yakushev et al., 2007)
Baan maximum specific growth rate	K_Baan_gro	d^{-1}	0.12	0.12 (Yakushev et al., 2007)
Baan specific rate of mortality	K_Baan_mrt	d^{-1}	1.2×10^{-2}	1.2×10^{-2} (Yakushev et al., 2007)
Bhan maximum specific growth rate	K_Bhan_gro	d^{-1}	0.19	0.19 (Yakushev et al., 2007)
Bhan specific rate of mortality	K_Bhan_mrt	d^{-1}	7×10^{-3}	7×10^{-3} (Yakushev et al., 2007)
Bhan increased specific rate of mortality due to O_2	K_Bhan_mrt_o2	d^{-1}	0.899	0.899 (Yakushev et al., 2007)
Limiting parameter for bacteria grazing by Het	limGrazBac	–	2	2 (Yakushev et al., 2007)
Limiting parameter for bacteria anaerobic heterotrophic	limBhan	–	2	2 (Yakushev et al., 2007)
Limiting parameter for bacteria aerobic heterotrophic	limBhae	–	5	5 (Yakushev et al., 2007)
Limiting parameter for bacteria anaerobic autotrophic	limBaan	–	2	2 (Yakushev et al., 2007)
Limiting parameter for nutrient consumption by Baae	limBaae	–	2	2 (Yakushev et al., 2007)
Phytoplankton				
Maximum specific growth rate	K_phy_gro	d^{-1}	4.8	0.9–1.3 (Savchuk, 2002), 3.0 (Gregoire and Lacroix, 2001)
Optimal irradiance	Iopt	$W\,m^{-2}$	25	50 (Savchuk, 2002)
1st coefficient for growth dependence on t	bm	$°C^{-1}$	0.12	0.12 (Burchard et al., 2006)
2nd coefficient for growth dependence on t	cm	–	1.4	1.4 (Burchard et al., 2006)
Specific rate of mortality	K_phy_mrt	d^{-1}	0.15	0.3–0.6 (Savchuk, 2002), 0.05 (Gregoire and Lacroix, 2001)
Specific rate of excretion	K_phy_exc	d^{-1}	0.05	0.01 (Burchard et al., 2006)
Heterotrophs				
Maximum specific rate of grazing of Het on Phy	K_het_ phy_gro	d^{-1}	1.0	0.9 (Gregoire and Lacroix, 2001), 1.5 (Burchard et al., 2006)
Half-saturation constant for the grazing of Het on Phy for Phy / Het ratio	K_het_phy_lim	–	1.1	1 (Yakushev et al., 2007)
Maximum specific rate of grazing of Het on POM	K_het_ pom_gro	d^{-1}	0.7	1.2 (Burchard et al., 2006)
Specific respiration rate	K_het_res	d^{-1}	0.02	1 (Yakushev et al., 2007)
Half-saturation constant for the grazing of Het on POM in dependence to ratio POM / Het	K_het_pom_lim	–	0.2	0.2 (Yakushev et al., 2007)
Maximum specific rate of mortality of Het	K_het_mrt	d^{-1}	0.05	0.05 (Gregoire and Lacroix, 2001)
Food absorbency for heterotrophs	Uz	–	0.5	0.5–0.7 (Savchuk, 2002)
Ratio between dissolved and particulate excretes of heterotrophs	Hz	–	0.5	0.5 (Gregoire and Lacroix, 2001)

Table 3. Continued.

(e)				
Parameter	Notation	Units	Value	Reference ranges
Rate of sinking of Phy	Vphy	$m\,d^{-1}$	1	0.1–0.5 (Savchuk, 2002)
Rate of sinking of Het	Vhet	$m\,d^{-1}$	1	1 (Yakushev et al., 2007)
Rate of sinking of bacteria (Bhae, Baae, Bhan, Baan)	Vbact	$m\,d^{-1}$	0.4	0.5 (Yakushev et al., 2007)
Rate of sinking of detritus (PON)	Vsed	$m\,d^{-1}$	6	0.4 (Savchuk, 2002), 1–370 (Alldredge and Gotschalk, 1988)
Rate of sinking of inorganic particles (Fe and Mn hydroxides, carbonates)	Vm	$m\,d^{-1}$	8	6–18 (Yakushev et al., 2007)

Table 4. Rates of biogeochemical production/consumption of the model compartments: **(a)** nutrients and oxygen; **(b)** Redox metals and sulfur; **(c)** carbon and alkalinity; **(d)** ecosystem parameters.

(a)	
Parameter	Rate
O_2	$R\,O_2 = (GrowthPhy - RespHet - DcDM\_O2 - DcPM\_O2) \times r\_o\_n - 0.25 \times mn\_ox1 - 0.25 \times mn\_ox2 - 0.25 \times fe\_ox1 - 0.5 \times hs\_ox - 0.5 \times s0\_ox\,0.5 \times s2o3\_ox - 0.5 \times mns\_ox - 1.5 \times Nitrif1 - 0.5 \times Nitrif2 - 2.25 \times fes\_ox - 3.5 \times fes2\_ox\,0.5 \times mnco3\_ox + feco3\_ox - 2 \times ch4\_o2$
Particulate organic nitrogen (PON)	$R\,PON = MortBaae + MortBaan + MortBhae + MortBhan + MortPhy + MortHet + Grazing \times (1 - Uz) \times (1 - Hz) - GrazPOP) - autolysis - DcPM\_O2 - DcPM\_NOX - DcPM\_SO4 - DcPM\_Mn - DcPM\_Fe - 0.5 \times DcPM\_CH4$
Dissolved organic nitrogen (DON)	$R\,DON = autolysis - DcDM\_O2 - DcDM\_NOX - DcDM\_SO4 - DcDM\_Mn - DcDM\_Fe - 0.5 \times DcPM\_CH4 - HetBhae - HetBhan + ExcrPhy + Grazing \times (1 - Uz) \times Hz$
NH_4	$R\,NH_4 = Dc\_OM\_total - Nitrif1 - anammox + 0.75 \times s0\_ox + s2o3\_ox - ChemBaae - ChemBaan + RespHet - GrowthPhy \times \frac{LimNH4}{LimN}$
NO_2	$R\,NO_2 = Nitrif1 - Nitrif2 + Denitr1 - Denitr2 - anammox - GrowthPhy \times \frac{LimNO3}{LimN} \times \frac{\mathbf{NO_2}}{\mathbf{NO_2}+\mathbf{NO_3}+10^{-5}}$
NO_3	$R\,NO_3 = Nitrif2 - Denitr1 - 1.6 \times hs\_no3 - 0.75\,s0\_ox - s2o3\_ox - GrowthPhy \times \left(\frac{LimNO_3}{LimN}\right) \times \left(\frac{\mathbf{NO_3}+10^{-5}}{\mathbf{NO_2}+\mathbf{NO_3}+10^{-5}}\right)$
PO_4	$R\,PO_4 = \frac{GrowthPhy+RespHet+Dc\_\_OM\_\_total-ChemBaae-ChemBaan}{r\_n\_p} + fe\_\_p\_\_compl + mn\_\_p\_\_compl$
Si	R Si= (ExcrPhy-GrowthPhy) × r_si_n +fe_si_compl
Si particulate	$R\,Si\,part = -K\_sipart\_diss \times \mathbf{Sipart} + (MortPhy + GrazPhy) \times r\_si\_n)$
(b)	
Parameter	Rate
Mn(II)	$R\,Mn2 = mn\_rd2 - mn\_ox1 + mns\_diss - mns\_form - mnco3\_form + mnco3\_diss + 0.5 \times fe\_ox2 + (DcDM\_Mn + DcPM\_Mn) \times r\_mn\_n$
Mn(III)	$R\,Mn3 = mn\_ox1 - mn\_ox2 + mn\_rd1\ mn\_rd2$
Mn(IV)	$RMn4 = mn\_ox2 - mn\_rd1 - 0.5 \times fe\_ox2 + mnco3\_ox - (DcDM\_Mn + DcPM\_Mn) \times r\_mn\_n$
MnS	$R\,MnS = mns\_form - mns\_diss$
$MnCO_3$	$R\,MnCO_3 = mnco3\_form - mnco3\_diss - mnco3\_ox$
Fe(II)	$R\,Fe2 = fe\_rd - fes\_form - fe\_ox1 - fe\_ox2 + fes\_diss - feco3\_form + feco3\_diss + fes2\_ox + 4 \times r\_fe\_n \times (DcDM\_Fe + DcPM\_Fe)$
Fe(III)	$R\,Fe3 = fe\_ox1 + fe\_ox2 - fe\_rd + fes\_ox + feco3\_ox - 4 \times r\_fe\_n \times (DcDM\_Fe + DcPM\_Fe)$
FeS	$R\,FeS = fes\_form - fes\_diss - fes\_ox - fes2\_form$
FeS_2	$R\,FeS_2 = fes2\_form - fes2\_ox$
$FeCO_3$	$R\,FeCO_3 = feco3\_form - feco3\_diss - feco3\_ox$
H_2S	$R\,H_2S = 0.5 \times s0\_disp - hs\_no3 + s2o3\_rd - fes2\_form - 0.5 \times mn\_rd1 - 0.5 \times mn\_rd2 - 0.5 \times fe\_rd - hs\_ox + fes\_diss - fes\_form + mns\_diss - mns\_form$
S^0	$R\,S^0 = hs\_ox + 0.5 \times mn\_rd1 + 0.5 \times mn\_rd2 + 0.5 \times fe\_rd - s0\_ox - s0\_disp - s\_no3$
S_2O_3	$R\,S_2O_3 = 0.5 \times s0\_ox - s2o3\_ox + 0.25 \times s0\_disp + 0.5 \times so4\_rd - 0.5 \times s2o3\_rd - s2o3\_no$
SO_4	$RSO_4 = hs\_no3 - so4\_rd + 0.5 \times s2o3\_ox + s\_no3 + 2 \times s2o3\_no3 + fes\_ox + 2 \times fes2\_ox$
(c)	
Parameter	Rate
DIC	$R\,DIC = caco3\_diss - caco3\_form - mnco3\_form + mnco3\_diss + mnco3\_ox - feco3\_form + feco3\_diss + feco3\_ox + (Dc\_OM\_total - ChemBaae - ChemBaan - GrowthPhy + RespHet) \times r\_c\_n$
$CaCO_3$	$R\,CaCO3 = caco3\_form - caco3\_diss$
CH_4	$R\,CH4 = ch4\_form - ch4\_ox$
Total alkalinity	$R\,Alk = dAlk$

Table 4. Continued.

(d)	
Parameter	Rate
Phytoplankton	RPhy = GrowthPhy − MortPhy − ExcrPhy − GrazPhy
Heterotrophs	RHet = Uz × Grazing − MortHet − RespHet
Aerobic heterotrophic bact.	RBhae = HetBhae − MortBhae − GrazBhae
Aerobic autotrophic bact.	RBaae = ChemBaae − MortBaae − GrazBaae
Anaerobic heterotrophic bact.	RBhan = HetBhan − MortBhan − GrazBhan
Anaerobic autotrophic bact.	RBaan = ChemBaan − MortBaan − GrazBaan

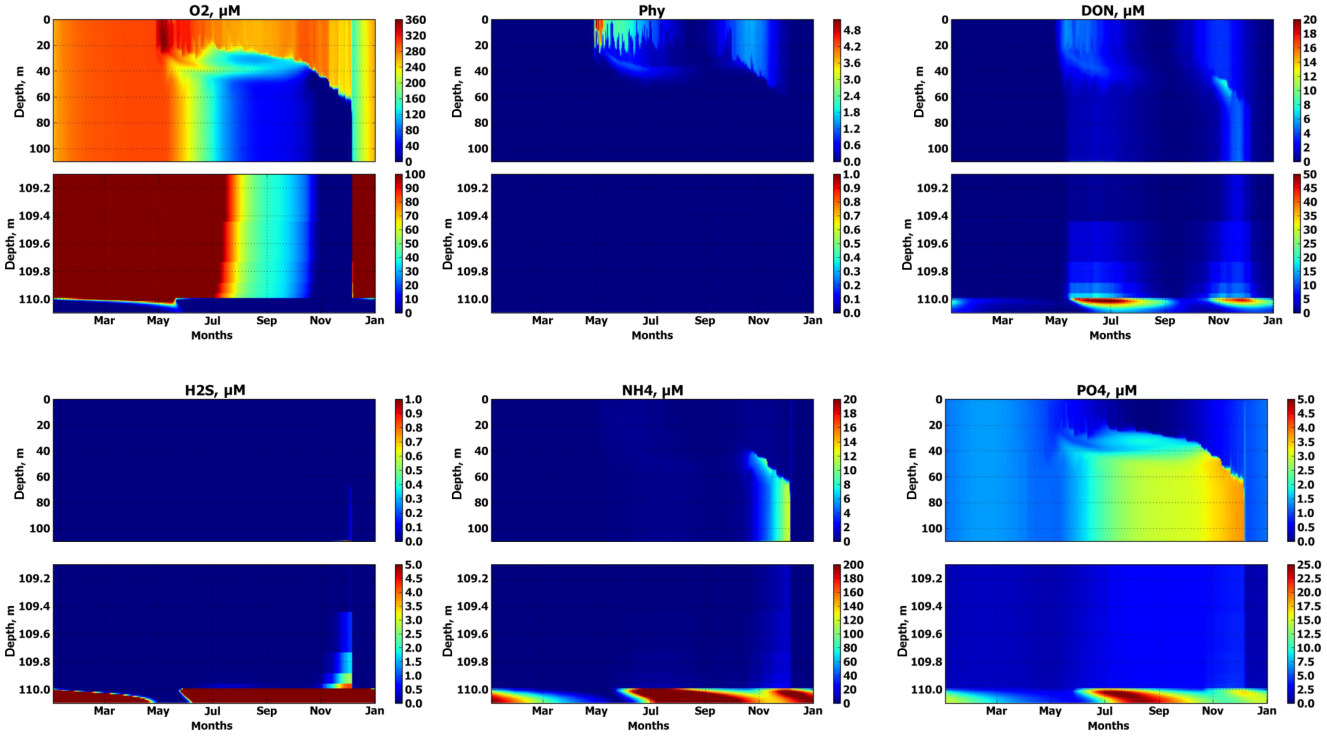

Figure 2. Simulated seasonal variability of the selected modeled chemical parameters (µM), in the water column (top panels) and in the benthic boundary layer and sediments (bottom panels).

the reactions of particles in the sediments are assumed to have negligible impact on the volume fraction of total solids, and the deep particulate burial velocity w_∞ in compacted sediments (where $\varphi = \varphi_\infty$) is assumed to be a known constant $w_{b\infty}$ (an input parameter). Since compaction ceases at this (possibly infinite) depth, the solute burial velocity must here equal the particulate burial velocity ($u_\infty = w_{b\infty}$). Steady state then implies the following burial velocities (Appendix B):

$$w = \frac{(1-\varphi_\infty)}{(1-\varphi)} w_{b\infty} - \frac{1}{(1-\varphi)} D_B^{\text{inter}} \frac{\partial \varphi}{\partial z} \quad (6)$$

$$u = \frac{\varphi_\infty}{\varphi} w_{b\infty} + \frac{1}{\varphi} D_B^{\text{inter}} \frac{\partial \varphi}{\partial z}, \quad (7)$$

where D_B^{inter} is the interphase bioturbation diffusivity, non-zero only at the SWI and only if bioturbation across the SWI is enabled. In the second approach, the reactions of the modeled particulate substances in the sediments modify the total solid volume fraction, and the modeled sinking fluxes from the water column modify the flux of solid volume at the SWI. The velocities in Eqs. (6) and (7) then define background velocities (w_b, u_b) due to non-modeled particulates. Assuming steady-state compaction leads to the following corrections to the background burial velocities (see Appendix B):

$$w' = \frac{1}{(1-\varphi)} \sum_i^{N_p} \frac{1}{\rho_i} \left[v_{f(i)} \hat{C}_{sf(i)} + \int_{z_{SWI}}^{z} R_i\left(z'\right) \mathrm{d}z' \right] \quad (8)$$

$$u' = \frac{1}{\varphi}\left(w'_{\infty} - (1-\varphi)\, w'\right), \tag{9}$$

where $w' = w - w_b$, $u' = u - u_b$, N_p is the number of particulate variables, ρ_i is the density of the ith particle type, $v_{f(i)}$ is the sinking velocity in the fluff layer, $\hat{C}_{sf(i)}$ is the suspended particulate concentration in the fluff layer, R_i is the particulate reaction term, and w'_{∞} is the correction to the deep particulate burial velocity, in practice approximated by the deepest value of w'. Since the suspended portion $\hat{C}_{sf(i)}$ is not explicitly modeled, it is approximated as the minimum of the particulate concentrations in the fluff layer and the layer immediately above. In our applications, we have found that Eqs. (8) and (9) can improve the realism of sediment organic matter distributions, mainly by increasing the burial rate following pelagic production and export events such as the spring bloom.

Finally, the process of bioirrigation, whereby benthic organisms flush out their burrows with water from the sediment surface, is modeled as a non-local solute exchange (following Aller, 2001; Meile et al., 2001; Rutgers Van Der Loeff and Boudreau, 1997; Schlüter et al., 2000):

$$T_{\mathrm{birr}C(i)} = \alpha\varphi \frac{O_{2s}}{O_{2s} + K_{O2s}} \left(\hat{C}_{f(i)} - C_i\right) \text{ (for solutes)}, \tag{10}$$

where $\alpha(z)$ is the bioirrigation rate in oxic conditions, $\hat{C}_{f(i)}$ is the flushing concentration of solute in the fluff layer, and the Michaelis–Menten function again accounts for the suppression of worm activity in anoxic conditions. The oxic bioirrigation rate $\alpha(z)$ is parameterized as an exponential decay from the sediment surface as in Schlüter et al. (2000). The total mass transfer to/from the sediment column must be balanced by a flux into/out of the fluff layer (see Eq. 1):

$$T_{\mathrm{birr}(i)} = \frac{1}{h_f} \frac{O_{2s}}{O_{2s} + K_{O2s}} \int_{z_{SWI}}^{z_{max}} \alpha\varphi \left(C_i - \hat{C}_{f(i)}\right) \mathrm{d}z' \quad \text{(for solutes)}, \tag{11}$$

where h_f is the thickness of the fluff layer and z_{max} is the depth of the bottom of the modeled sediment column. $T_{\mathrm{birr}C(i)}, T_{\mathrm{birr}(i)} = 0$ for all particulate variables.

2.1.7 BROM-transport numerical integration

Equations (1)–(3) are integrated numerically over a single combined grid (water column plus sediments) and using the same model time step in both water column and sediments. All concentrations are stored internally and input/output in units [mmol m^{-3} total volume]. Time stepping follows an operator splitting approach (Butenschön et al., 2012): concentrations are successively updated by contributions over one time step of diffusion, bioirrigation, reaction, and sedimentation, in that order. If any state variable has any "not-a-number" values at the end of the time step then the program is terminated.

Diffusive updates are calculated either by a simple forward-time central-space (FTCS) algorithm or by a semi-implicit central-space algorithm adapted from a routine in the General Ocean Turbulence Model, GOTM (Umlauf et al., 2005). Bioirrigation and reaction updates are calculated from forward Euler time steps, using FABM to compute R_i, and sedimentation updates are calculated using a simple first-order upwind differencing scheme. After each update, Dirichlet boundary conditions (see below) are reimposed and all concentrations are low bounded by a minimum value (default = 10^{-11} µM) to avoid negative values. Maximum diffusive and advective Courant numbers can optionally be output after every time step or when/if a not-a-number value is detected. Before starting the integration, the program calculates Courant numbers due to eddy/molecular diffusion and returns a warning message if maximum values on any given day exceed 0.5 and the FTCS option is selected.

BROM-transport also provides an option to divide the diffusion and sedimentation updates into smaller time steps related to the sources-minus-sinks time step by fixed factors, since the physical transport processes are often numerically limiting (Butenschön et al., 2012). The default time step is 0.0025 days or 216 s, which is much longer than the characteristic equilibration timescale of the CO_2 kinetics (Zeebe and Wolf-Gladrow, 2001).

2.1.8 BROM-transport vertical grid

The vertical grid in BROM-transport is divided into the pelagic water column, the BBL, and the sediments. The pelagic water column grid is either set as uniform with height/spacing set by the brom.yaml file (see Sect. S1 in the Supplement), or it is read from the NetCDF forcing input file (see below), with an option to decrease resolution by subsampling. In principle, the NetCDF input from the hydrodynamic model may already include a fully resolved BBL, but in practice we find this is rarely the case. BROM-transport therefore allows the user to "insert" a high-resolution BBL into the bottom of the input water column. This BBL has non-uniform grid spacing with layer thickness decreasing geometrically towards the SWI, reaching O (cm) thickness for the fluff layer, based on parameters from the brom.yaml file. For the upper sediments, the layer thickness is increased geometrically moving down from the SWI, from O (mm) thickness in the surface layer to O (cm) thickness deeper in the sediments, again based on brom.yaml parameters. The result is a full grid with non-uniform spacing and maximum resolution near the SWI. As in many ocean models (e.g., ROMS, GOTM) the vertical grid in BROM-transport is staggered: temperature, salinity, and biogeochemical concentrations are defined at layer midpoints, while diffusivities, sinking/burial velocities, and resulting transport fluxes are all defined on layer interfaces.

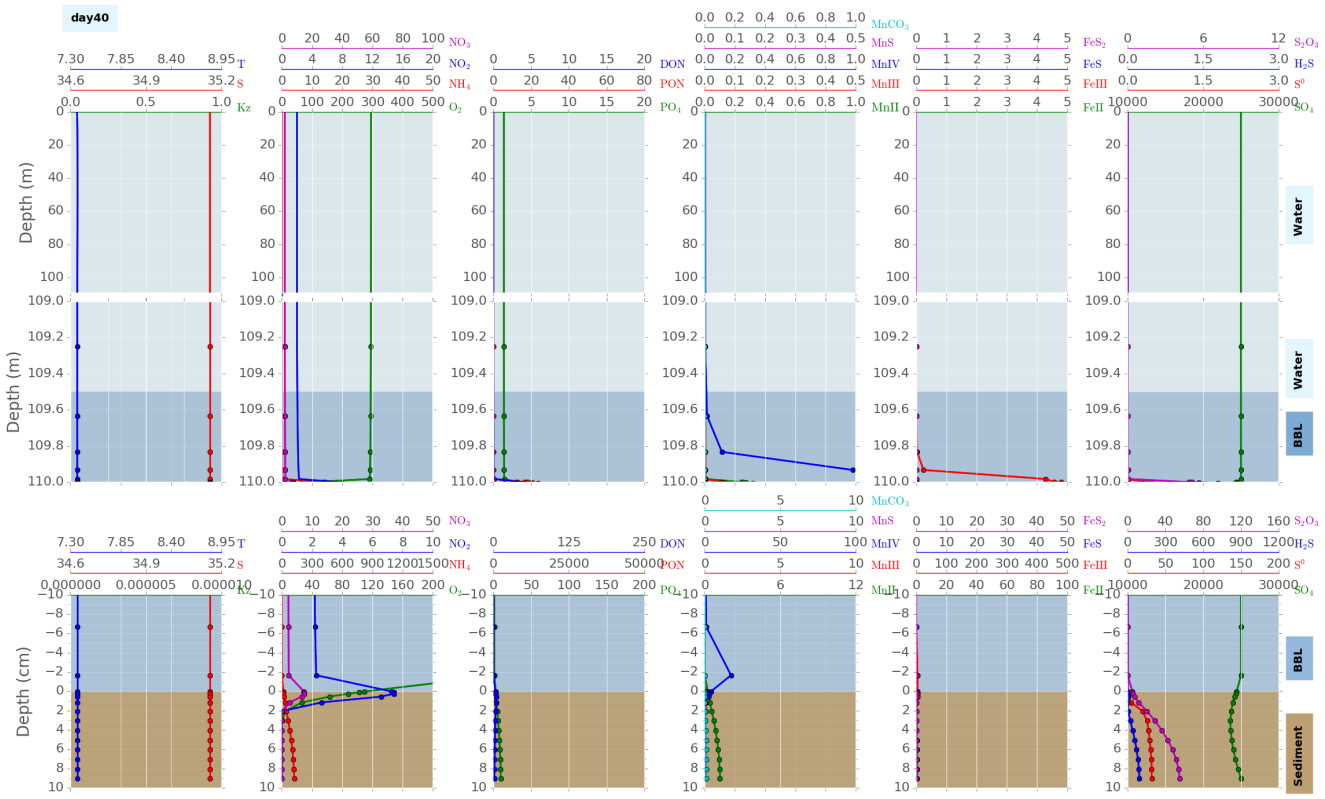

Figure 3.

2.1.9 BROM-transport initial conditions

Initial conditions for all concentrations in Eqs. (1)–(3) can be provided by either using the initialization values defined in the fabm.yaml file (see Sect. S2 in the Supplement) as uniform initial conditions for each variable, or by providing the initial conditions for all variables at every depth in a text file with a specific format. Typically, these initial-condition text files are generated by running the model to a steady state annual cycle and saving the final values as the desired start date. Alternatively, they could be generated by interpolating/smoothing data, in which case the user should note that the input concentrations must be in units [mmol m^{-3} total volume].

2.1.10 BROM-transport boundary conditions

BROM-transport presently allows the user to choose between four different types of boundary conditions for each variable and for upper and lower boundaries: (1) no gradient at the bottom boundary (no diffusive flux) or no flux at the surface boundary, except where parameterized by the FABM biogeochemical model (i.e., for O_2 and DIC in the case of BROM-biogeochemistry); (2) a fixed constant value; (3) a fixed sinusoidal variation in time defined by amplitude, mean value, and phase parameters; or (4) an arbitrary fixed variation in time read from the input NetCDF file. All boundary condition options and parameters are set in the brom.yaml file (see Sect. S1). Note that options 2–4 are Dirichlet boundary conditions which define implicit fluxes of matter into and out of the model domain, and that all boundary concentrations should be in units [mmol m^{-3} total volume (water+solids)]. The default option 1 is generally the preferred choice, but the Dirichlet options can also be useful to allow a simple representation of, e.g., fluxes of nutrients into and out of the surface layer due to lateral riverine input. A possible alternative is to use the forcings' parameters for horizontal mixing (see Eq. 1) to specify horizontal exchanges or restoring terms to observed climatology (see Sect. 2.2.7).

Under option 1, and using BROM-biogeochemistry, a surface O_2 flux representing exchange with the atmosphere is parameterized as

$$Q_{O_2} = K_{660} \times \left(\frac{Sc}{660}\right)^2 \times (O_{2sat} - O_2)\,, \tag{12}$$

where O_{2sat} is the oxygen saturation as a function of temperature and salinity, according to UNESCO (1986), Sc is the Schmidt number for oxygen (Raymond et al., 2012), and k_{660} is the reference gas-exchange transfer velocity, parameterized as $k_{660} = 0.365\,u^2 + 0.46\,u$ (Schneider et al., 2002) where u is the wind speed 10 m above the

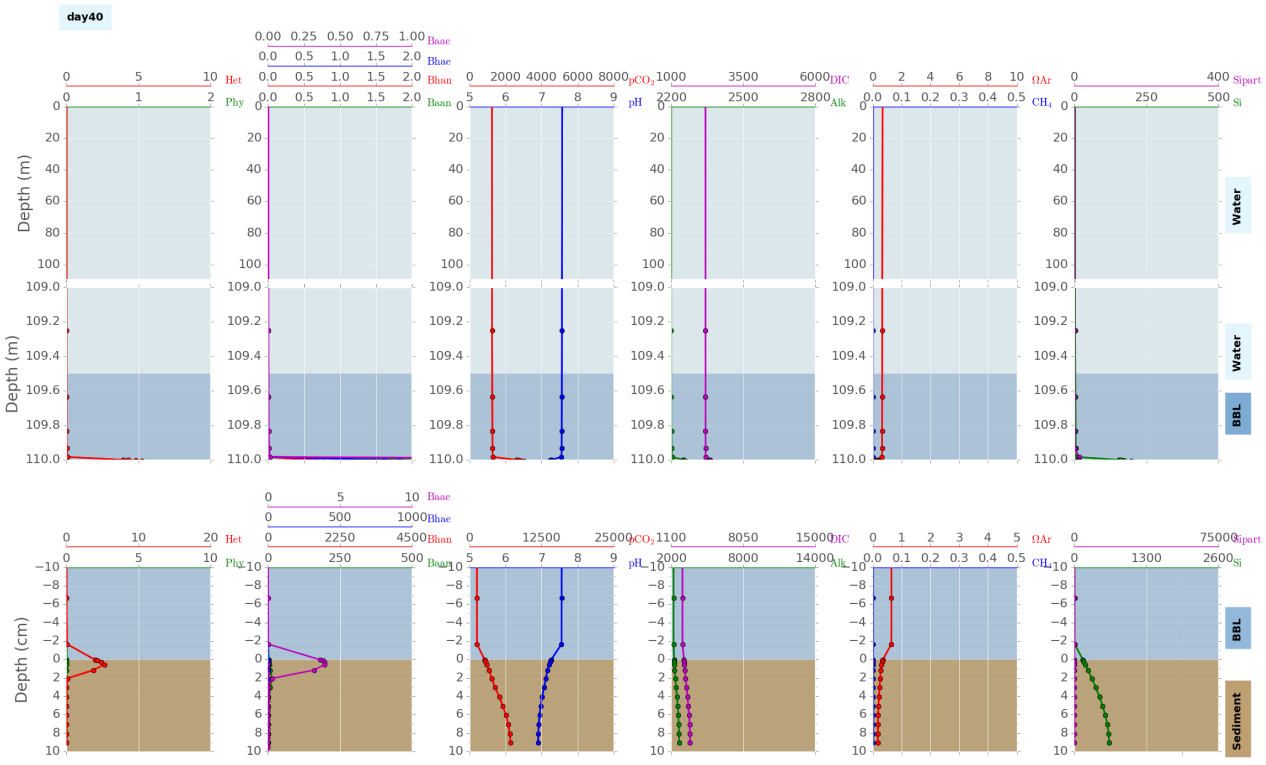

Figure 3. Vertical distributions of the modeled chemical parameters (µM), biological parameters (µM N), temperature (°C), salinity (PSU), and vertical diffusivity (10^{-3} m^2 s^{-1}) during the winter period of well-mixed conditions, showing the water column (light blue), the benthic boundary layer (dark blue), and the sediments (light brown). Vertical distributions of the modeled chemical parameters (µM) and biological parameters (µM N) during the winter period of well-mixed conditions, showing the water column (light blue), the benthic boundary layer (dark blue), and the sediments (light brown).

sea surface (m s^{-1}). Air–sea exchange of CO_2 in BROM-biogeochemistry is parameterized using the partial pressures in water (pCO_2^{water}) and air (pCO_2^{air}) following the formulation and coefficients in Butenschön et al. (2016):

$$Q_{O_2} = F_{wind} \times \left(pCO_2{}^{air} - pCO_2{}^{water} \right), \quad (13)$$

where $F_{wind} = (0.222\,u^2 + 0.333\,u)(Sc/660)^{-0.5}$ is a wind parameter (Nightingale et al., 2000), u is the wind speed, and Sc is the Schmidt number for CO_2 (Raymond et al., 2012).

2.1.11 BROM-transport irradiance model

BROM-transport includes two simple Beer–Lambert attenuation models to calculate in situ 24 h average photosynthetically active radiation (PAR) as needed by BROM-biogeochemistry and many other biogeochemical models. The first is derived from the current ERSEM default model (Blackford et al., 2004; Butenschön et al., 2016) and models the total attenuation as

$$k_t = k_0 + k_{Phy}\mathrm{Phy} + k_{PON}\mathrm{PON} + k_s S, \quad (14)$$

where k_0 is the background attenuation of seawater, k_{Phy} and k_{PON} are the specific attenuations due to phytoplankton and detritus, respectively, and k_s is the specific attenuation due to "other" optically active substances with concentration S (currently a constant input parameter). The second model includes attenuation due to other optically active concentrations that are modeled by BROM-biogeochemistry:

$$k_t = k_0 + k_{Phy}\mathrm{Phy} + k_{PON}\mathrm{PON} + k_{Het}\mathrm{Het} + k_{DON}\mathrm{DON} + k_{PB}\,B + k_{PIV}\mathrm{PIV} + k_s S, \quad (15)$$

where B is the total bacterial concentration (Baae + Baan + Bhae + Bhan) and PIV is the total volume fraction of modeled inorganic particles, calculated from the concentrations using input densities of each inorganic solid. The final irradiance is scaled by a constant parameter representing either the photosynthetically active fraction of the in situ irradiance or the relationship between surface PAR in water and the forcing surface irradiance (Mobley and Boss, 2012). The forcing surface irradiance Eair(t) can be read from NetCDF input or otherwise calculated using a sinusoidal function (Yakushev et al., 2013b). In addition, the surface attenuation due to ice cover can be accounted for as a simple linear function of a NetCDF input ice thickness variable hice(t).

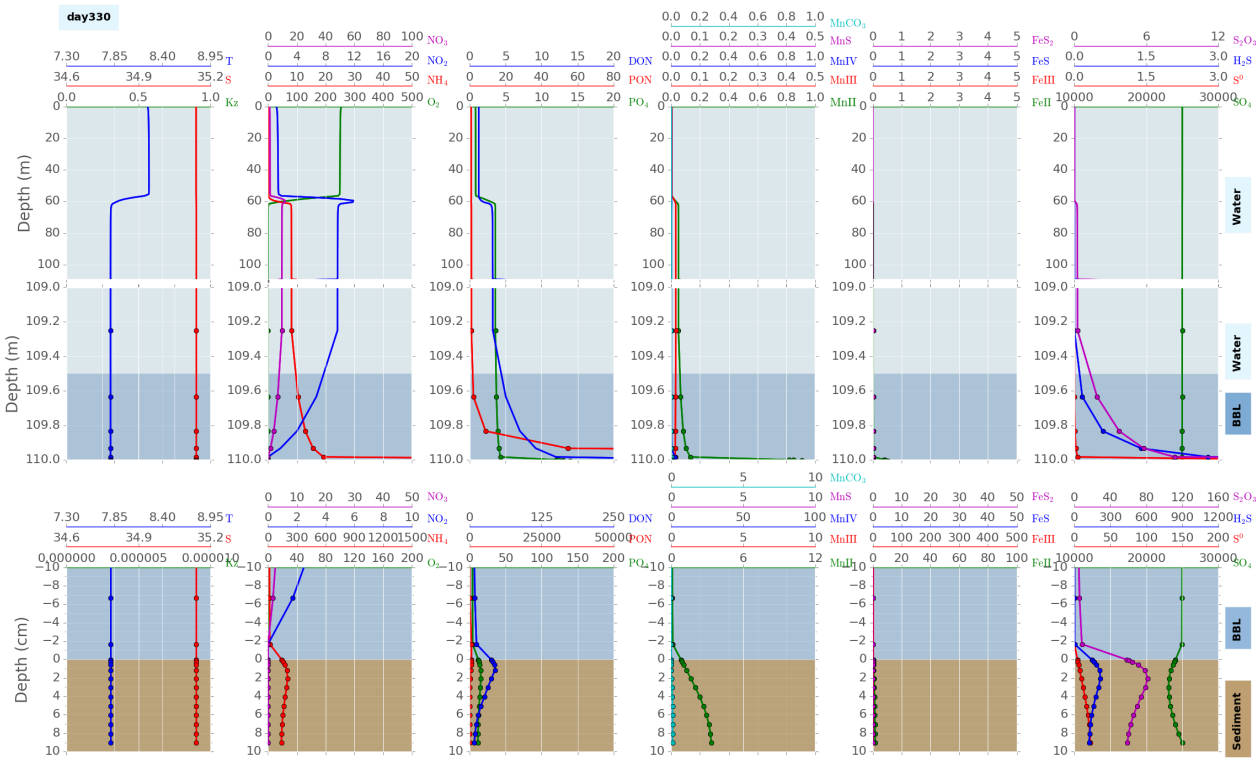

Figure 4.

2.1.12 BROM-transport input forcings

BROM-transport requires forcing inputs at least for temperature, salinity, and vertical diffusivity at all depths in the pelagic water column and for each day of the simulation. These may be provided from an input subroutine that creates simple, hypothetical profiles, or from text/NetCDF files containing data from interpolations of measurements or hydrodynamic model output. Forcing time series of surface irradiance and ice thickness may also be read as NetCDF input. BROM-transport then uses these inputs in combination with parameters set in the runtime input file brom.yaml (see Sect. S1) to solve the transport-reaction equations on a "full" vertical grid including pelagic water column, BBL, and sediment subgrids.

In order to run, BROM-transport must extend the input pelagic (temperature, salinity, diffusivity) forcings over the full grid. Temperature and salinity in the BBL and sediments are set as uniform and equal to the values at the bottom of the input pelagic water column for each day. The vertical diffusivity needs a more careful treatment, as it is the main defining characteristic of the pelagic vs. BBL vs. sediment environments. Within the water column, the total vertical diffusivity $D = D_m + D_e$ for solutes and $D = D_e$ for particulates, where D_m is a constant molecular diffusivity at infinite dilution, and D_e is the eddy diffusivity read from the input file for the pelagic water column. For the BBL, D_e can be defined as "dynamic", in which case it is linearly interpolated for each day between the deepest input forcing value above the SWI and zero at a depth h_{DBL} above the SWI, where h_{DBL} is the diffusive boundary layer (DBL) thickness (default value 0.5 mm). This option is likely appropriate for shallow-water applications where D_e may be strongly time dependent within the user-defined BBL (default thickness 0.5 m). Alternatively, a static, fixed profile $D_{eBBL}(z)$ may be more appropriate for deep-water BBLs, where time dependence may be weak and deepest values from hydrodynamic models may be relatively far above the SWI. In this case, BROM-transport offers two options for $D_{eBBL}(z)$: (1) a constant value, dropping to zero in the DBL, or (2) a linear variation between a fixed value at the top of the BBL and zero at the top of the DBL. Option 1 defines a simplest-possible assumption, while option 2 corresponds to the assumption of a log layer for the current speed (e.g., Boudreau and Jorgensen, 2001; Holtappels and Lorke, 2011). Eddy diffusivity is strictly zero in the DBL, on the SWI, and within the sediments. Diffusivity in the sediments is due to molecular diffusion and bioturbation and is parameterized as described in Sect. 2.2.1.

Optional forcings for BROM-transport include 24 h average surface irradiance Eair(t), which is often supplied by hydrodynamic models (e.g., ROMS), a surface ice thickness forcing hice(t), and depth–time arrays of horizontal mixing rates $\varepsilon_h(z,t)$ and horizontal mixing concentrations $\hat{C}_{0i}(z,t)$

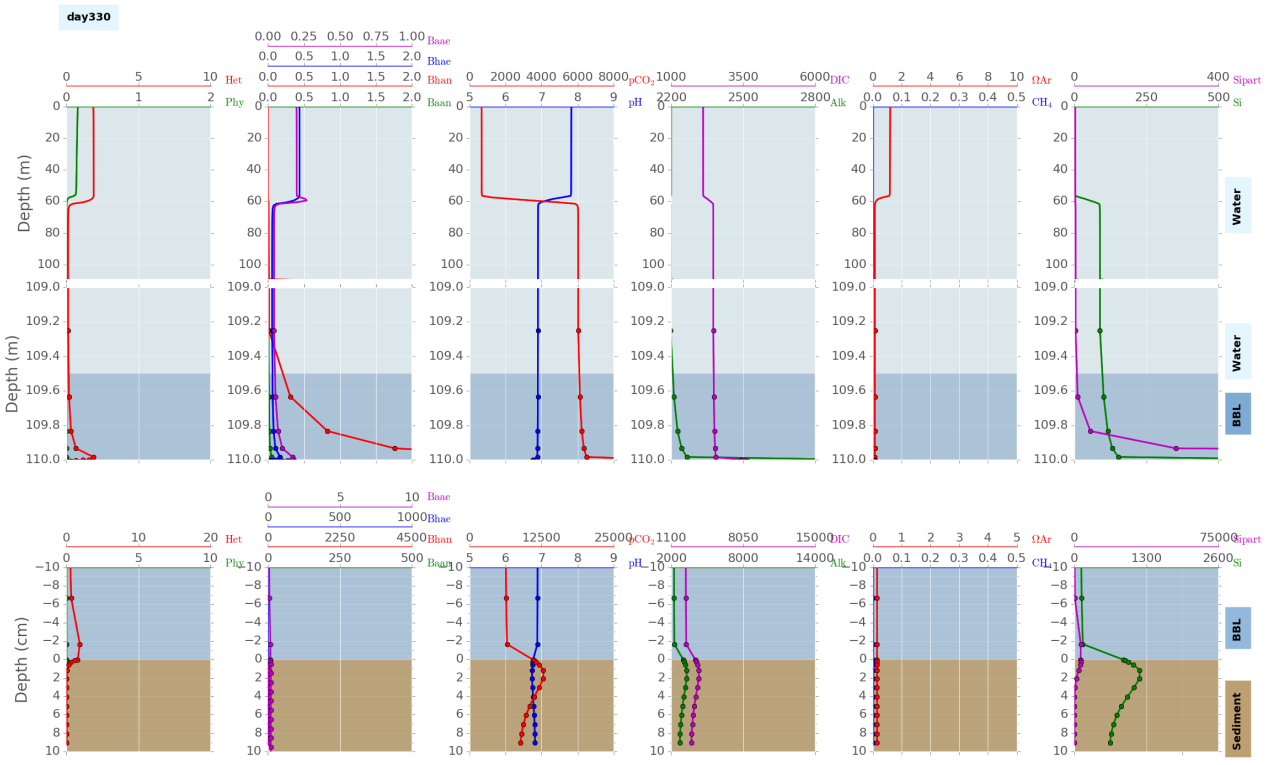

Figure 4. Vertical distributions of the modeled chemical parameters (µM), biological parameters (µM N), temperature (°C), salinity (PSU), and vertical diffusivity (10^{-3} m^2 s^{-1}) during the period of bottom anoxia, showing the water column (light blue), the benthic boundary layer (dark blue), and the sediments (light brown). Vertical distributions of the modeled chemical parameters (µM) and biological parameters (µM N) during the period of bottom anoxia, showing the water column (light blue), the benthic boundary layer (dark blue), and the sediments (light brown).

(see Eq. 1). Horizontal mixing rates within the inserted BBL and sediments are set to zero. Note that these horizontal mixing forcings can also be used to define relaxation or restoring fluxes to climatological values within the pelagic water column, which may in some cases provide a valid means of accounting for horizontal flux divergence effects that are missing in the 1-D model.

3 BROM demonstration run

3.1 Model setup

A North Sea hydrodynamic scenario was used to demonstrate the ability of BROM to reproduce the biogeochemical mechanisms of oxic/anoxic transformations. Complete lists of the model options and parameter values used are given in Sect. S1 (brom.yaml input file for BROM-transport) and Sect. S2 (fabm.yaml input file for BROM-biogeochemistry).

The BROM-transport water column extended from 0 to 110 m, with a pelagic spatial resolution of 1 m inherited from the GOTM hydrodynamic model used to provide forcings. A high-resolution BBL was inserted from 109.5 to 110 m, with layer thickness decreasing from approximately 25 to 3 cm in the fluff layer. Sediment grid points were added to cover the upper 10 cm of sediments with layer thickness increasing from 0.5 mm in the surface layer to 1 cm at depth. This choice of grid does not explicitly resolve the DBL (default thickness 0.5 mm) but the main DBL function of limiting solute exchange between the BBL and sediments is largely fulfilled by the fluff layer (thickness 3 cm) and upper sediment layer (thickness 0.5 mm). The model time step for BROM-transport was set to 0.0025 days (216 s).

Upper boundary conditions included sinusoidal, time-varying Dirichlet boundary conditions for nitrate, phosphate, and silicate, implying net influxes and outfluxes of surface nutrients, as well as the default parameterized air–sea fluxes of O_2 and DIC (see Sect. S1). Lower boundary conditions assumed (by default) zero diffusive flux for all reduced components (i.e., hydrogen sulfide, solid-phase concentrations of metal sulfides and carbonates, silicon, and OM). The simulation therefore focuses on the consequences of the supply of fresh OM as a main reducer in both water column and sediments.

The pelagic water column was forced by output from a GOTM hydrodynamical simulation for temperature, salinity, and vertical diffusivity (taken from the salinity diffusivity)

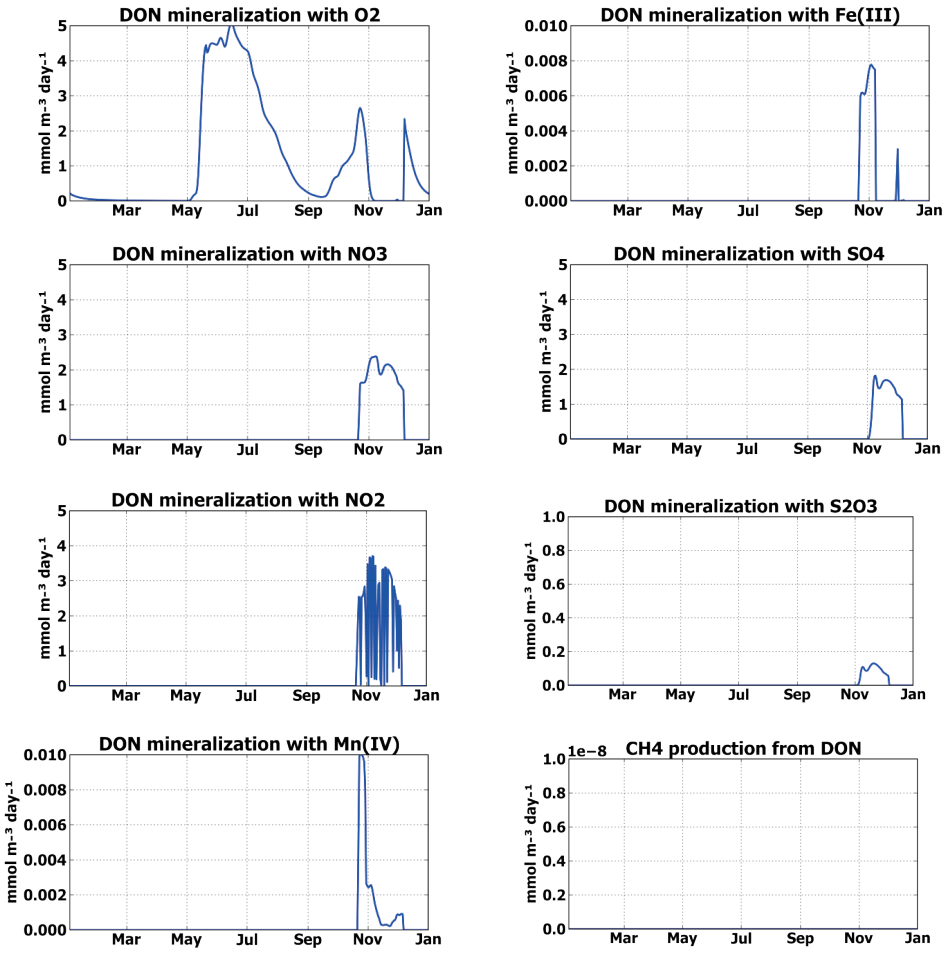

Figure 5. Simulated seasonal variability of biogeochemical transformation rates just above the sediment water interface, showing the rates of DON mineralization with oxygen, nitrate, nitrite, Mn(IV), Fe(III), SO_4, S_2O_3, and CH_4 production from DON. Units are in mmol m^{-3} d^{-1}.

and surface irradiance calculated using the sinusoidal option. We aimed for a solution representative of "present day" and therefore treated the GOTM forcing as representative of a "normal year". BROM-transport was spun up from vertically homogeneous initial conditions for 100 model years with repeated-year forcings and boundary conditions. After this time, a quasi-stationary solution with seasonally forced oscillations of the biogeochemical variables had been reached.

The results of these calculations were written to an output file in NetCDF format, including the daily vertical distributions of model state variables, diagnostic rates of biogeochemical transformations, and fluxes associated with diffusion and sedimentation. This output can be visualized by any NetCDF-compatible software.

3.2 Results

The model simulated the periodic replacement of oxic with anoxic conditions in the BBL following seasonal mixing and OM production. The simulation demonstrates the characteristic features of biogeochemical profiles in the water column, BBL, and upper sediments, as well as their variability under changing redox conditions (Figs. 2–4).

During intensive mixing conditions in winter, the water column is well oxygenated and the oxic/anoxic interface is located at a depth of several centimeters in the sediments (Figs. 2, 3). In summer, just after the spring bloom, an enrichment of the sediment surface with fresh OM and a restricted oxygen supply leads to the consumption of O_2 by OM mineralization and close to suboxic conditions (Fig. 2). The second bloom in autumn leads to a further decrease of oxygen concentrations to complete depletion. There is a concomitant increase in reduced forms of N, Mn, and Fe, and finally of hydrogen sulfide in the bottom water (Figs. 2, 4). The redox interface thus moves from the sediment to the BBL.

Figure 5 shows the rate of OM mineralization with a variety of electron acceptors. Oxygen is consumed during OM mineralization in summer and autumn and, after its complete depletion, denitrification dominates, with both nitrate reduction and nitrite reduction playing significant roles. The rate

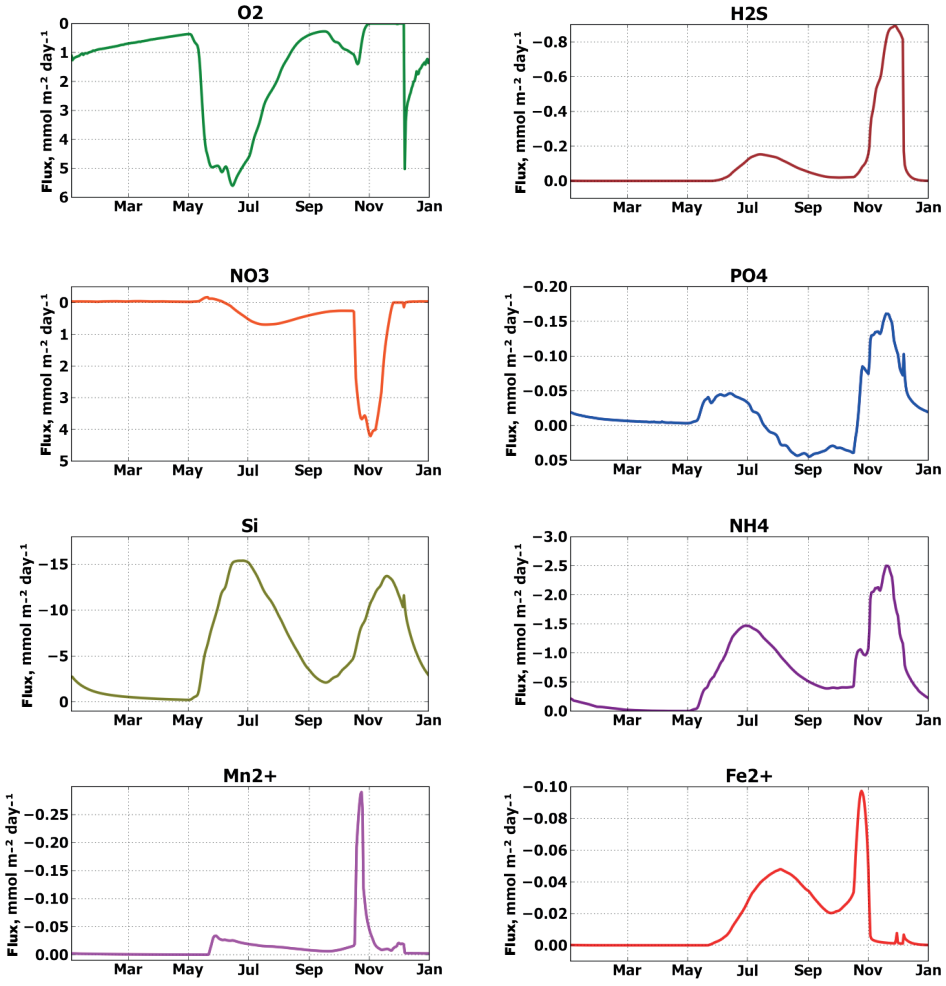

Figure 6. Simulated seasonal variability of vertical diffusive fluxes from the benthic boundary layer to the sediments of oxygen, hydrogen sulfide, nitrate, silicate, ammonia, Mn(II), and Fe(II). Positive fluxes are downward and negative fluxes are upward. Units are in mmol m^{-2} d^{-1}.

of mineralization of OM with Mn and Fe oxides is small, but as these processes prevent mineralization with sulfate, they cause a lag of a few days between the depletion of oxygen and the appearance of hydrogen sulfide in the water column (Figs. 2, 5). The amount of labile degradable OM is relatively small and mineralization with sulfate completely removes the remaining OM, thus preventing methanogenesis (Fig. 5).

The seasonal variability of the sediment–water fluxes clearly demonstrates the appearance in the bottom water of reduced forms of N, Mn, Fe, and phosphate (Fig. 6).

Generally, the concentrations, vertical distributions, and benthic–pelagic fluxes of the parameters considered in the model are reasonable and are within observed ranges for the North Sea (Queirós et al., 2014) and some other regions with temporary bottom anoxia (Almroth et al., 2009; McCarthy et al., 2008; Morse and Eldridge, 2007; Pakhomova et al., 2007; Queirós et al., 2014; Yu et al., 2015).

4 Conclusion and future work

This paper presents a description of BROM, a fully coupled pelagic–benthic model that provides an integrated framework to study the biogeochemistry of a water column and upper sediments. BROM simulates changes in redox conditions and their impact on the distributions of a wide range of biogeochemical variables. In particular, BROM provides a detailed description of the fate and availability of dissolved oxygen and hydrogen sulfide: the former essential for macroscopic marine life, the latter highly toxic to it. BROM can therefore provide valuable information to ecological studies, particularly in the context of multistressor impacts. The model suggests that the timing of hydrogen sulfide release into the pelagic is linked to the dynamics of several electron acceptors that are themselves of limited interest for biogeochemical and ecological purposes, and that are therefore rarely included in models. The ability of BROM to simulate and forecast H_2S toxicity is in fact the direct result of its inclusion of

several of these rarely modeled chemical compounds (e.g., Mn(IV), Fe(III)).

This paper was not devoted to a detailed validation of BROM with in situ data; we plan to explore this in future work. A qualitative analysis of the model results (Sect. 3) suggests that the model can produce realistic distributions and fluxes of key biogeochemical variables during periodic changes in redox conditions.

In summary, we present a new benthic–pelagic biogeochemical model (BROM) that combines a relatively simple pelagic ecosystem model with a detailed biogeochemical model of the coupled cycles of N, P, Si, C, O, S, Mn, and Fe in the water column, benthic boundary layer, and sediments, with a focus on oxygen and redox state. BROM should be of interest for the study a range of environmental applications in addition to hypoxia, such as benthic nutrient recycling, redox biogeochemistry, eutrophication, industrial pollution from trace elements, organic loading, and ocean acidification.

5 Code availability

The model as presented consists of two components. The first is a set of biogeochemical modules (brom/redox, brom/bio, brom/carb, brom/eqconst), available as part of the official FABM distribution (http://fabm.net); BROM-specific files are located in subdirectory src/models/niva/brom). The second is a hydrophysical driver (BROM-transport) that provides the 1-D vertical context and resolves transport; this is available separately from https://github.com/e-yakushev/brom-git.git. When combined, the 1-D BROM model as presented is obtained.

Both FABM and BROM-transport are coded in object-oriented Fortran 2003, have a build system based on CMake (https://cmake.org), and use YAML files (http://yaml.org) for runtime configuration. The code is platform independent and only requires a Fortran 2003-capable compiler, e.g., gfortran 4.7 or higher, or the Intel Fortran compiler version 12.1 or higher. BROM-transport includes facilities for producing results as NetCDF files, which can be read by a variety of software on different platforms.

Also, you can run BROM without any Fortran compiler using a Win32 executable file (which can be downloaded from https://github.com/e-yakushev/brom-git/releases/tag/v1.1).

As BROM's biogeochemical modules are built on FABM, they can be used from a wide range of 1-D and 3-D hydrodynamic models, including GOTM, GETM, ROMS, MOM, NEMO, and FVCOM (a ROMS-FABM coupler has been developed by P. Wallhead; NEMO-FABM and FVCOM-FABM couplers have been developed by the Plymouth Marine Laboratory; contact J. Bruggeman for information).

Results shown in this paper were produced with BROM-transport tag v1.1 and the BROM-biogeochemistry code in FABM tag v0.95.3, available from the above repositories. The simulation was run using the netCDF/.yaml input files found in the data folder of the BROM-transport repository. However, we envisage BROM to be further developed in a backward compatible manner, and encourage users to adopt the latest version of the code. Step-by-step instructions for running BROM are found in Appendix A. Both FABM and BROM-transport are distributed under the GNU General Public License (http://www.gnu.org/licenses/). As a component of FABM, BROM-biogeochemistry is licensed under the same conditions as FABM.

Appendix A: Running BROM step by step

1. Installation requires a Fortran 2003-capable compiler, e.g., gfortran 4.7 or higher, or the Intel Fortran compiler version 12.1 or higher. In our demonstration, we used the Intel Fortran Compiler version 15.0.4.221. Additionally, a NetCDF library compatible with the chosen Fortran compiler is required. CMake software should be installed. After ensuring these prerequisites are in place, create a directory to hold the BROM model code and associated input and output files. Detailed instructions for installation are provided at the BROM repository (https://github.com/e-yakushev/brom-git.git).

2. Preparation of input files consists of the model reading two .yaml files with the model parameters (fabm.yaml and brom.yaml), as well as a NetCDF or text file with the hydrophysical forcing data. Optionally, the biogeochemical initial conditions can be read from a text file **start.dat**; this may be a file written by a previous simulation (the final model state is written to a file named **finish.dat** at the end of every simulation).

   i. The brom.yaml (see Sect. S1) file specifies the values of transport model parameters as well as various option switches and input/output file and variable names. Text comments provide guidance and references for setting parameter values. If using NetCDF input, the user should pay careful attention to the NetCDF input parameters and names, ensuring that this information is consistent with the input NetCDF file. The selected-year parameter year must refer to a year that is covered by the input forcing data.

   ii. The fabm.yaml (see Sect. S2) file specifies the values of biogeochemical model parameters, default initial values for state variables, and the coupling of FABM modules. Text comments provide annotation and references.

   iii. The nns_annual.nc (in the example) file contains input forcing data that may be derived from observations or hydrodynamical model output (GOTM in our demonstration). It can be replaced by a text (.dat) file if this is the format of the hydrodynamical model output.

   iv. The start.dat is the text file with initial values for model state variables at every depth. This file may be created by renaming the output of a previous simulation (finish.dat is the state on 1 January of the last modeled year).

3. Output files are NetCDF and headed text files generated automatically by the model during the simulation. Output files can be readily imported into various software packages for visualization and further analysis. Certain output files (Vertical_grid.dat and Hydrophysics.dat) are generated early in the simulation and should be checked by the user to ensure that the model grid and hydrophysical forcings are set up as intended.

   i. Vertical_grid.dat is the text file with model layer indices, midpoint depths, increments between midpoint depths, and thicknesses.

   ii. Hydrophysics.dat is the text file with daily profiles of hydrophysical variables (temperature, salinity, diffusivity, porosity, tortuosity, burial velocities).

   iii. The finish.dat is the text file with the state variables for the 1 January of the last modeled year. It can be used for visualization or as initial conditions for further calculations.

   iv. The output_NNday.dat is the optional text file with the state variables and diagnostic variables for day NN to make plots of vertical distributions (e.g., Fig. 3)

   v. BROM_out.nc is the NetCDF file with daily profiles of state variables, rates of biogeochemical transformations, and vertical fluxes.

4. For visualization of NetCDF output files, any software with NetCDF input can be used. In the example, we used PyNcView for 2-D and BROM_pictures for 1-D (available at https://github.com/BottomRedoxModel/brom_pictures).

Appendix B: Derivation of burial velocities

The conservation equations for liquid and total solid volume fractions in the sediments can be written as

$$\frac{\partial \varphi}{\partial t} = \frac{\partial}{\partial z} D_{\mathrm{B}}^{\mathrm{inter}} \frac{\partial \varphi}{\partial z} - \frac{\partial}{\partial z} u\varphi - \sum\nolimits_{i=1}^{N_{\mathrm{p}}} \rho_i^{-1} R_i \tag{B1}$$

$$\frac{\partial (1-\varphi)}{\partial t} = \frac{\partial}{\partial z} D_{\mathrm{B}}^{\mathrm{inter}} \frac{\partial (1-\varphi)}{\partial z} - \frac{\partial}{\partial z} w (1-\varphi) + \sum\nolimits_{i=1}^{N_{\mathrm{p}}} \rho_i^{-1} R_i, \tag{B2}$$

where $D_{\mathrm{B}}^{\mathrm{inter}}$ is the interphase bioturbation diffusivity (possibly non-zero only at the SWI), ρ_i is the density of the ith particulate substance, and R_i is the corresponding reaction term. Equations (B1) and (B2) assume that the densities of liquid and total solid are both constant, and they retain the net contributions of reactive terms although these are often considered negligible, e.g., (Boudreau, 1997; Meysman et al., 2005). Summing Eqs. (B1) and (B2) and integrating over depth gives a useful and quite general relationship:

$$\varphi u + (1-\varphi) w = U, \tag{B3}$$

where $U(t)$ is only a function of time. If we now assume no externally impressed porewater flow, it follows that at some (possibly infinite) depth where compaction ceases ($\frac{\partial \varphi}{\partial z} = 0$,

$\varphi = \varphi_\infty$), the solute burial velocity u must here equal the particulate burial velocity w, hence $u_\infty = w_\infty$. Equation (B3) becomes

$$\varphi u + (1-\varphi)\, w = w_\infty. \tag{B4}$$

Now assuming steady state compaction ($\frac{\partial \varphi}{\partial t} = 0$), Eq. (B2) can be integrated from the SWI to a depth z within the sediments:

$$(1-\varphi) w + D_{\mathrm{B}}^{\mathrm{inter}} \frac{\partial \varphi}{\partial z} = (1-\varphi_{\mathrm{SWI}})\, w_{\mathrm{SWI}} + D_{\mathrm{BSWI}}^{\mathrm{inter}} \frac{\partial \varphi}{\partial z}_{\mathrm{SWI}} + \sum\nolimits_i^{N_\mathrm{p}} \frac{1}{\rho_i} \int_{z_{\mathrm{SWI}}}^{z} R_i\left(z'\right) \mathrm{d}z'. \tag{B5}$$

To determine the first term on the right-hand side of Eq. (B5), we assume that the total solid volume flux across the SWI is equal to the total solid volume flux from the sinking of suspended particulate matter in the fluff layer:

$$(1-\varphi_{\mathrm{SWI}}) w_{\mathrm{SWI}} + D_{\mathrm{BSWI}}^{\mathrm{inter}} \frac{\partial \varphi}{\partial z}_{\mathrm{SWI}} = F_{\mathrm{b}} + \sum\nolimits_i^{N_\mathrm{p}} \frac{1}{\rho_i} v_{\mathrm{f}(i)} \hat{C}_{\mathrm{sf}(i)}, \tag{B6}$$

where F_{b} defines a constant background solid volume flux due to non-modeled particles, $v_{\mathrm{f}(i)}$ is the sinking velocity in the fluff layer, and $\hat{C}_{\mathrm{sf}(i)}$ is the suspended particulate concentration in the fluff layer. Substituting into Eq. (B5), we have

$$(1-\varphi) w + D_{\mathrm{B}}^{\mathrm{inter}} \frac{\partial \varphi}{\partial z} = F_{\mathrm{b}} + \sum\nolimits_i^{N_\mathrm{p}} \frac{1}{\rho_i} \left[v_{\mathrm{f}(i)} \hat{C}_{\mathrm{sf}(i)} + \int_{z_{\mathrm{SWI}}}^{z} R_i\left(z'\right) \mathrm{d}z' \right]. \tag{B7}$$

Since $D_{\mathrm{B}}^{\mathrm{inter}} \frac{\partial \varphi}{\partial z}$ is zero at depth, the constant surface flux term is given by $F_{\mathrm{b}} = (1-\varphi_\infty)\, w_{\mathrm{b}\infty}$, where both φ_∞ and $w_{\mathrm{b}\infty}$ are input parameters. Hence, we have

$$(1-\varphi) w + D_{\mathrm{B}}^{\mathrm{inter}} \frac{\partial \varphi}{\partial z} = (1-\varphi_\infty)\, w_{\mathrm{b}\infty} + \sum\nolimits_i^{N_\mathrm{p}} \frac{1}{\rho_i} \left[v_{\mathrm{f}(i)} \hat{C}_{\mathrm{sf}(i)} + \int_{z_{\mathrm{SWI}}}^{z} R_i\left(z'\right) \mathrm{d}z' \right]. \tag{B8}$$

Equation (6) directly follows from Eq. (B8) by neglecting the modeled settling flux and reaction terms, then Eq. (7) follows by application of Eq. (B4). Equations (8) and (9) follow by considering the additional particulate burial velocity due to fluxes and reactions (from the last term in Eq. B8) and applying Eq. (B4) to obtain the additional solute burial velocity.

The Supplement related to this article is available online at doi:10.5194/gmd-10-453-2017-supplement.

Author contributions. Development of the model code was made by E. V. Yakushev, E. A. Protsenko, J. Bruggeman, P. Wallhead, and S. Yakubov; analyses of the model results and discussions were conducted by R. G. J. Bellerby, R.-M. Couture, and S. V. Pakhomova; and all authors contributed to the writing of the manuscript.

Acknowledgements. We wish to thank J. Middelburg, O. P. Savchuk, and G. Munhoven for detailed and constructive reviews that led to a greatly improved manuscript. We acknowledge funding from the EC 7th Framework Program (FP7/2007-2013) under grant agreement no. 265847 ("Sub-seabed CO2 Storage: Impact on Marine Ecosystems", ECO2) and 240837 ("Research into Impacts and Safety in CO2 Storage", RISCS), EC Horizon 2020 under grant agreement no. 654462 ("STrategies for Environmental Monitoring of Marine Carbon Capture and Storage", STEMM-CCS), with additional development funds from FME SUCCESS; CO2Base; EEA CO2MARINE; Norwegian Research Council projects no. 236658 ("New knowledge on sea deposits", NYKOS), no. 535640 ("Combined effects of multiple organic stressors from jellyfish blooms and aquaculture operations on seafloor ecosystems", JELLYFARM), and no. 254777 (Environmental impacts of leakage from sub-seabed CO2 storage, Trykk CO2); the Research Council of Norway through its Centers of Excellence funding scheme, project number 223268/F50 (CERAD), contract no. 208279 (NIVA Strategic Institute Initiative "Climate effects from Mountains to Fjords"); NIVA OASIS; and VISTA – a basic research program and collaborative partnership between the Norwegian Academy of Science and Letters and Statoil, project no. 6164. The work of J. Bruggeman was funded by NERC National Capability in Marine Modeling. R.-M. Couture acknowledges funding by RCN project no. 244558.

Edited by: D. Roche
Reviewed by: O. P. Savchuk, G. Munhoven, and J. Middelburg

References

Alldredge, A. L. and Gotschalk, C.: In situ settling behavior of marine snow, Limnol. Oceanogr., 33, 339–35, doi:10.4319/lo.1988.33.3.0339, 1988.

Aller, R. C.: Transport and reactions in the bioirrigated zone, in: The Benthic Boundary Layer: Transport Processes and Biogeochemistry, edited by: Boudreau, B. and Jørgensen, B. B., Oxford Press, 2001.

Almroth, E., Tengberg, A., Andersson, J. H., Pakhomova, S., and Hall, P. O. J.: Effects of resuspension on benthic fluxes of oxygen, nutrients, dissolved inorganic carbon, iron and manganese in the Gulf of Finland, Baltic Sea, Cont. Shelf Res., 29, 807–818, doi:10.1016/j.csr.2008.12.011, 2009.

Anderson, J. J., Okubo, A., Robbins, A. S., and Richards, F. A.: A model for nitrite and nitrate distributions in oceanic oxygen minimum zones, Deep-Sea Res., 29, 1113–1140, 1982.

Arndt, S. and Regnier, P.: A model for the benthic-pelagic coupling of silica in estuarine ecosystems: sensitivity analysis and system scale simulation, Biogeosciences, 4, 331–352, doi:10.5194/bg-4-331-2007, 2007.

Bektursunova, R. and L'Heureux, I.: A reaction-transport model of periodic precipitation of pyrite in anoxic marine sediments, Chem. Geol., 287, 158–170, doi:10.1016/j.chemgeo.2011.06.004, 2011.

Berner, R. A.: Principles of Chemical Sedimentology, McGraw-Hill Inc., 1971.

Berner, R. A. Early Diagenesis: A Theoretical Approach, Princeton Series in Geochemistry, 1, 241 pp., 1980.

Blackford, J. C., Allen, J. I., and Gilbert, F. J.: Ecosystem dynamics at six contrasting sites: A generic modelling study, J. Marine Syst., 52, 191–215, doi:10.1016/j.jmarsys.2004.02.004, 2004.

Blackwelder, P., Hood, T., Alvarez-Zarikian, C., Nelsen, T. A., and McKee, B.: Benthic foraminifera from the necop study area impacted by the Mississippi River plume and seasonal hypoxia, Quarternary Int., 31, 19–36, doi:10.1016/1040-6182(95)00018-E, 1996.

Boudreau, B. P.: A method-of-lines code for carbon and nutrient diagenesis in aquatic sediments, Comput. Geosci., 22, 479–496, doi:10.1016/0098-3004(95)00115-8, 1996.

Boudreau, B. P.: Diagenetic models and their implementation, Modelling transport and reactions in aquatic sediments, doi:10.1007/978-3-642-60421-8, 1997.

Boudreau, B. P. and Jorgensen, B. B.: The Benthic Boundary Layer: Transport Processes and Biogeochemistry, edited by: Boudreau, B. P. and Jorgensen, B. B., Oxford University Press, 1st Edn., 2001.

Brezonik, P. L. and Arnold, W. A.: Water Chemistry An Introduction to the Chemistry of Natural and Engineered Aquatic Systems, Oxford University Press, New York, 1st Edn., 2011.

Brigolin, D., Lovato, T., Rubino, A., and Pastres, R.: Coupling early-diagenesis and pelagic biogeochemical models for estimating the seasonal variability of N and P fluxes at the sediment-water interface: Application to the northwestern Adriatic coastal zone, J. Marine Syst., 87, 239–255, doi:10.1016/j.jmarsys.2011.04.006, 2011.

Bruggeman, J. and Bolding, K.: A general framework for aquatic biogeochemical models, Environ. Modell. Softw., 61, 249–265, doi:10.1016/j.envsoft.2014.04.002, 2014.

Burchard, H., Bolding, K., Kühn, W., Meister, A., Neumann, T., and Umlauf, L.: Description of a flexible and extendable physical-biogeochemical model system for the water column, J. Marine Syst., 61 (3–4 Spec. Iss.), 180–211, doi:10.1016/j.jmarsys.2005.04.011, 2006.

Butenschön, M., Zavatarelli, M., and Vichi, M.: Sensitivity of a marine coupled physical biogeochemical model to time resolution, integration scheme and time splitting method, Ocean Model., 52–53, 36–53, doi:10.1016/j.ocemod.2012.04.008, 2012.

Butenschön, M., Clark, J., Aldridge, J. N., Allen, J. I., Artioli, Y., Blackford, J., Bruggeman, J., Cazenave, P., Ciavatta, S., Kay, S., Lessin, G., van Leeuwen, S., van der Molen, J., de Mora, L., Polimene, L., Sailley, S., Stephens, N., and Torres, R.: ERSEM 15.06: a generic model for marine biogeochemistry and the

ecosystem dynamics of the lower trophic levels, Geosci. Model Dev., 9, 1293–1339, doi:10.5194/gmd-9-1293-2016, 2016.

Canfield, D. E., Thamdrup, B., and Kristensen, E.: Aquatic geomicrobiology, in: Advances in Marine Biology, edited by: Southward, A. J., Tyler, P. A., Young, C. M., and Fuiman, L. A., Elsevier Academic Press, Amsterdam, vol. 48, 640 pp., 2005.

Cerco, C. F., Noel, M. R., and Kim, S.-C.: Three-dimensional Management Model for Lake Washington, Part II: Eutrophication Modeling and Skill Assessment, Lake Reserv. Manage., 22, 115–131, doi:10.1080/07438140609353889, 2006.

Cooper, D. C. and Morse, J. W.: The Chemistry of Offatts Bayou, Texas: A Seasonally Highly Sulfidic Basin, Estuaries, 19, 595, doi:10.2307/1352520, 1996.

Couture, R. M., Shafei, B., Van Cappellen, P., Tessier, A., and Gobeil, C.: Non-steady state modeling of arsenic diagenesis in lake sediments, Environ. Sci. Technol., 44, 197–203, doi:10.1021/es902077q, 2010.

Dade, W. B., Hogg, A. J., and Boudreau, B. P.: Physics of Flow Above the Sediment-Water Interface, in: The Benthic Boundary Layer, edited by: Boudreau, B. P. and Jorgensen, B. B., Oxford University Press, New York, 4–43, 2001.

Davison, W.: Iron and manganese in lakes, Earth-Sci. Rev., 34, 119–163, 1993.

Debolskaya, E. I., Yakushev, E. V., and Kuznetsov, I. S.: Analysis of the hydrophysical structure of the Sea of Azov in the period of the bottom anoxia development, J. Marine Syst., 70, 300–307, doi:10.1016/j.jmarsys.2007.02.027, 2008.

Diaz, R. J. and Rosenberg, R.: Spreading dead zones and consequences for marine ecosystems, Science, 321, 926–929, doi:10.1126/science.1156401, 2008.

Dickson, A. G.: The development of the alkalinity concept in marine chemistry, Mar. Chem., 40, 49–63, doi:10.1016/0304-4203(92)90047-E, 1992.

Fennel, K., Hetland, R., Feng, Y., and DiMarco, S.: A coupled physical-biological model of the Northern Gulf of Mexico shelf: model description, validation and analysis of phytoplankton variability, Biogeosciences, 8, 1881–1899, doi:10.5194/bg-8-1881-2011, 2011.

Glud, R. N.: Oxygen dynamics of marine sediments, Mar. Biol. Res., 4, 243–289, doi:10.1080/17451000801888726, 2008.

Gregoire, M. and Lacroix, G.: Study of the oxygen budget of the Black Sea waters using a 3D coupled hydrodynamical – biogeochemical model, J. Marine Syst., 31, 175–202, doi:10.1016/S0924-7963(01)00052-5, 2001.

He, Y., Stanev, E. V., Yakushev, E., and Staneva, J.: Black Sea biogeochemistry: Response to decadal atmospheric variability during 1960–2000 inferred from numerical modeling, Mar. Environ. Res., 77, 90–102, doi:10.1016/j.marenvres.2012.02.007, 2012.

Holtappels, M. and Lorke, A.: Estimating turbulent diffusion in a benthic boundary layer, Limnol. Oceanogr.-Meth, 9, 29–41, doi:10.4319/lom.2011.9.29, 2011.

Hunter, K. S., Wang, Y., and Van Cappellen, P.: Kinetic modeling of microbially-driven redox chemistry of subsurface environments: coupling transport, microbial metabolism and geochemistry, J. Hydrol., 209, 53–80, doi:10.1016/S0022-1694(98)00157-7, 1998.

Jensen, D. L., Boddum, J. K., Tjell, J. C., and Christensen, T. H.: The solubility of rhodochrosite (MnCO3) and siderite (FeCO3) in anaerobic aquatic environments, Appl. Geochem., 17, 503–511, doi:10.1016/S0883-2927(01)00118-4, 2002.

Jorgensen, B., Bang, M., and Blackburn, T.: Anaerobic mineralization in marine sediments from the Baltic Sea-North Sea transition, Mar. Ecol. Prog. Ser., 59, 39–54, doi:10.3354/meps059039, 1990.

Jourabchi, P., Van Cappellen, P., and Regnier, P.: Quantitative interpretation of pH distributions in aquatic sediments: A reaction-transport modeling approach, Am. J. Sci., 305, 919–956, doi:10.2475/ajs.305.9.919, 2005.

Jourabchi, P., Meile, C., Pasion, L. R., and Van Cappellen, P.: Quantitative interpretation of pore water O_2 and pH distributions in deep-sea sediments, Geochim. Cosmochim. Ac., 72, 1350–1364, doi:10.1016/j.gca.2007.12.012, 2008.

Kamyshny, A., Yakushev, E., Jost, G., and Podymov, O.: Chemical Structure of Pelagic Redox Interfaces, in: The Handbook of Environmental Chemistry, edited by: Yakushev, E., Springer Berlin Heidelberg, 2013.

Katsev, S., Sundby, B., and Mucci, A.: Modeling vertical excursions of the redox boundary in sediments: Application to deep basins of the Arctic Ocean, Limnol. Oceanogr., 51, 1581–1593, doi:10.4319/lo.2006.51.4.1581, 2006.

Katsev, S., Chaillou, G., Sundby, B., and Mucci, A.: Effects of progressive oxygen depletion on sediment diagenesis and fluxes: A model for the lower St. Lawrence River Estuary, Limnol. Oceanogr., 52, 2555–2568, doi:10.4319/lo.2007.52.6.2555, 2007.

Konovalov, S. K., Murray, J. W., Luther, G. W., and Tebo, B. M.: Processes controlling the redox budget for the oxic/anoxic water column of the Black Sea, Deep. Res. Pt. II., 53, 1817–1841, doi:10.1016/j.dsr2.2006.03.013, 2006.

Lancelot, C., Spitz, Y., Gypens, N., Ruddick, K., Becquevort, S., Rousseau, V., Lacroix, G., and Billen, G.: Modelling diatom and Phaeocystis blooms and nutrient cycles in the Southern Bight of the North Sea: The MIRO model, Mar. Ecol. Prog. Ser., 289, 63–78, doi:10.3354/meps289063, 2005.

Lee, J. Y., Tett, P., Jones, K., Jones, S., Luyten, P., Smith, C., and Wild-Allen, K.: The PROWQM physical-biological model with benthicpelagic coupling applied to the northern North Sea, J. Sea Res., 48, 287–331, doi:10.1016/S1385-1101(02)00182-X, 2002.

Lewis, E. and Wallace, D.: Program developed for CO_2 system calculations, 4735, 1–21, 1998.

Lopes, F., Viollier, E., Thiam, A., Michard, G., Abril, G., Groleau, A., Prévot, F., Carrias, J.-F., Albéric, P., and Jézéquel, D.: Biogeochemical modelling of anaerobic vs. aerobic methane oxidation in a meromictic crater lake (Lake Pavin, France), Appl. Geochem., 26, 1919–1932, doi:10.1016/j.apgeochem.2011.06.021, 2011.

Luff, R. and Moll, A.: Seasonal dynamics of the North Sea sediments using a three-dimensional coupled sediment-water model system, Cont. Shelf Res., 24, 1099–1127, doi:10.1016/j.csr.2004.03.010, 2004.

Luff, R., Haeckel, M. and Wallmann, K.: Robust and fast FORTRAN and MATLAB libraries to calculate pH distributions in marine systems, Comput. Geosci., 27, 157–169, doi:10.1016/S0098-3004(00)00097-2, 2001.

McCarthy, M. J., McNeal, K. S., Morse, J. W., and Gardner, W. S.: Bottom-water hypoxia effects on sediment-water interface nitrogen transformations in a seasonally hypoxic, shallow bay

(Corpus Christi Bay, TX, USA), Estuar. Coasts, 31, 521–531, doi:10.1007/s12237-008-9041-z, 2008.

Meile, C., Koretsky, C. M., and Van Cappellen, P.: Quantifying bioirrigation in aquatic sedimnets: An inverse modeling approach, Limnol. Oceanogr., 1, 164–177, 2001.

Meire, L., Soetaert, K. E. R., and Meysman, F. J. R.: Impact of global change on coastal oxygen dynamics and risk of hypoxia, Biogeosciences, 10, 2633–2653, doi:10.5194/bg-10-2633-2013, 2013.

Meysman, F. J. R., Boudreau, B. P., and Middelburg, J. J.: Modeling reactive transport in sediments subject to bioturbation and compaction, Geochim. Cosmochim. Ac., 69, 3601–3617, doi:10.1016/j.gca.2005.01.004, 2005.

Millero, F. J.: Thermodynamics of the carbon dioxide system in the oceans, Geochim. Cosmochim. Ac., 59, 661–677, doi:10.1016/0016-7037(94)00354-O, 1995.

Mobley, C. D. and Boss, E. S.: Improved irradiances for use in ocean heating, primary production, and photo-oxidation calculations, Appl. Optics, 51, 6549–6560, doi:10.1364/AO.51.006549, 2012.

Morgan, J. J.: Manganese and its role in biological processes, in: Metal ions in biological systems, edited by: Sigel, A. and Sigel, H. Marcel Dekker, Inc., Basel, New York, 31, 1–30, 2000.

Morse, J. W. and Eldridge, P. M.: A non-steady state diagenetic model for changes in sediment biogeochemistry in response to seasonally hypoxic/anoxic conditions in the "dead zone" of the Louisiana shelf, Mar. Chem., 106, 239–255, doi:10.1016/j.marchem.2006.02.003, 2007.

Munhoven, G.: Mathematics of the total alkalinity–pH equation – pathway to robust and universal solution algorithms: the SolveSAPHE package v1.0.1, Geosci. Model Dev., 6, 1367–1388, doi:10.5194/gmd-6-1367-2013, 2013.

Nightingale, P. D., Malin, G., Law, C. S., Watson, A. J., Liss, P. S., Liddicoat, M. I., Boutin, J., and Upstill-Goddard, R. C.: In situ evaluation of air-sea gas exchange parameterizations using novel conservative and volatile tracers, Global Biogeochem. Cy., 14, 373–387, doi:10.1029/1999GB900091, 2000.

Pakhomova, S. V., Hall, P. O. J., Kononets, M. Y., Rozanov, A. G., Tengberg, A., and Vershinin, A. V.: Fluxes of iron and manganese across the sediment-water interface under various redox conditions, Mar. Chem., 107, 319–331, doi:10.1016/j.marchem.2007.06.001, 2007.

Paraska, D. W., Hipsey, M. R., and Salmon, S. U.: Sediment diagenesis models: Review of approaches, challenges and opportunities, Environ. Model. Softw., 61, 297–325, doi:10.1016/j.envsoft.2014.05.011, 2014.

Pavlidou, A., Kontoyiannis, H., Anagnostou, C., Siokou–Frangou, I., Pagou, K., Krasakopoulou, E., Assimakopoulou, G., Zervoudaki, S., Zeri, C., Chatzianestis, J., and Psyllidou-Giouranovits, R.: Biogeochemical Characteristics in the Elefsis Bay (Aegean Sea, Eastern Mediterranean) in Relation to Anoxia and Climate Changes, in: The Handbook of Environmental Chemistry, edited by: Yakushev, E., 161–201, Springer Berlin Heidelberg, 2013.

Pearson, T. H. and Rosenberg, R.: Macrobenthic succession in relation to organic enrichment and pollution of the marine environment, Oceanogr. Mar. Biol. Ann. Rev., 16, 229–311, doi:10.1111/j.1540-5834.2012.00707.x, 1978.

Popova, E. E. and Srokosz, M. A.: Modelling the ecosystem dynamics at the Iceland-Faeroes Front: Biophysical interactions, J. Marine Syst., 77, 182–196, doi:10.1016/j.jmarsys.2008.12.005, 2009.

Queirós, A. M., Norling, K., Amaro, T., Nunes, J., Cummings, D., Yakushev, E., Sorensen, K., Harris, C., Woodward, M., Danovaro, R., Rastelli, E., Alve, E., Vittor, C. De, Karuza, A., Cibic, T., Monti, M., Ingrosso, G., Fornasaro, D., Beaubien, S. E., Guilini, K., Vanreu, A., Bigalke, N., and Widdicombe, S.: Potential impact of CCS leakage on marine communities, Technical Report, Deliverable 4.1: Potential impact of CCS leakage on marine communitiesWP4; lead beneficiary: Plymouth Marine Laboratory, 2014.

Rabalais, N. N., Turner, R. E., and Scavia, D.: Beyond Science into Policy: Gulf of Mexico Hypoxia and the Mississippi River, Bioscience, 52, 129, doi:10.1641/0006-3568(2002)052[0129:BSIPGO]2.0.CO;2, 2002.

Raymond, P. A., Zappa, C. J., Butman, D., Bott, T. L., Potter, J., Mulholland, P., Laursen, a. E., McDowell, W. H., and Newbold, D.: Scaling the gas transfer velocity and hydraulic geometry in streams and small rivers, Limnol. Oceanogr. Fluids Environ., 2, 41–53, doi:10.1215/21573689-1597669, 2012.

Reed, D. C., Slomp, C. P., and Gustafsson, B. G.: Sedimentary phosphorus dynamics and the evolution of bottom-water hypoxia: A coupled benthic-pelagic model of a coastal system, Limnol. Oceanogr., 56, 1075–1092, doi:10.4319/lo.2011.56.3.1075, 2011.

Richards, F.: Anoxic basins and fjords, in: Chemical Oceanography, edited by: Riley, J. and Skirrow, G., Academic Press, London, 611–645, 1965.

Richardson, K. and Jørgensen, B.: Eutrophication: Definition, history and effects, in: Eutrophication in Coastal Marine Ecosystems, doi:10.1029/CE052p0001, 1996.

Rickard, D. and Luther, G. W.: Kinetics of pyrite formation by the H2S oxidation of iron (II) monosulfide in aqueous solutions between 25 and 125°C: The mechanism, Geochim. Cosmochim. Ac., 61, 135–147, doi:10.1016/S0016-7037(96)00322-5, 1997.

Roden, E. E. and Tuttle, J. H.: Sulfide release from estuarine sediments underlying anoxic bottom water, Limnol. Oceanogr., 37, 725–738, doi:10.4319/lo.1992.37.4.0725, 1992.

Roy, R. N., Roy, L. N., Vogel, K. M., Porter-Moore, C., Pearson, T., Good, C. E., Millero, F. J., and Campbell, D. M.: The dissociation constants of carbonic acid in seawater at salinities 5 to 45 and temperatures 0 to 45°C, Mar. Chem., 44, 249–267, doi:10.1016/0304-4203(93)90207-5, 1993.

Rutgers Van Der Loeff, M. M. and Boudreau, B. P.: The effect of resuspension on chemical exchanges at the sediment-water interface in the deep sea – A modelling and natural radiotracer approach, J. Marine Syst., 11, 305–342, doi:10.1016/S0924-7963(96)00128-5, 1997.

Savchuk, O. and Wulff, F.: Biogeochemical Transformations of Nitrogen and Phosphorus in the Environment, Coupling Hydrodynamic and Biogeochemical Processes in Models for the Baltic Proper, 2, 79 pp., 1996.

Savchuk, O. P.: Nutrient biogeochemical cycles in the Gulf of Riga: Scaling up field studies with a mathematical model, J. Marine Syst., 32, 253–280, doi:10.1016/S0924-7963(02)00039-8, 2002.

Schippers, A. and Jorgensen, B. B.: Biogeochemistry of pyrite and iron sulfide oxidation in marine sediments, Geochim. Cos-

mochim. Ac., 66, 85–92, doi:10.1016/S0016-7037(01)00745-1, 2002.

Schlüter, M., Sauter, E., Hansen, H. P., and Suess, E.: Seasonal variations of bioirrigation in coastal sediments: Modelling of field data, Geochim. Cosmochim. Ac., 64, 821–834, doi:10.1016/S0016-7037(99)00375-0, 2000.

Schneider, B., Nausch, G., Kubsch, H., and Petersohn, I.: Accumulation of total CO_2 during stagnation in the Baltic Sea deep water and its relationship to nutrient and oxygen concentrations, Mar. Chem., 77, 277–291, doi:10.1016/S0304-4203(02)00008-7, 2002.

Sell, K. S. and Morse, J. W.: Dissolved Fe2+ and $\sum$H2S Behavior in Sediments Seasonally Overlain by Hypoxic-to-anoxic Waters as Determined by CSV Microelectrodes, Aquat. Geochem., 12, 179–198, doi:10.1007/s10498-005-4574-2, 2006.

Sen Gupta, B. K., Turner, R. E., and Rabalais, N. N.: Seasonal oxygen depletion in continental-shelf waters of Louisiana: Historical record of benthic foraminifers, Geology, 24, 227–230, doi:10.1130/0091-7613(1996)024<0227:SODICS>2.3.CO;2, 1996.

Soetaert, K. and Middelburg, J. J.: Modeling eutrophication and oligotrophication of shallow-water marine systems: The importance of sediments under stratified and well-mixed conditions, Hydrobiologia, 629, 239–254, doi:10.1007/s10750-009-9777-x, 2009.

Soetaert, K., Herman, P. M. J., and Middelburg, J. J.: A model of early diagenetic processes from the shelf to abyssal depths, Geochim. Cosmochim. Ac., 60, 1019–1040, doi:10.1016/0016-7037(96)00013-0, 1996.

Soetaert, K., Middelburg, J. J., Herman, P. M. J., and Buis, K.: On the coupling of benthic and pelagic biogeochemical models, Earth-Science On the coupling of benthic and pelagic biogeochemical models, April 2016, 173–201, doi:10.1016/S0012-8252(00)00004-0, 2000.

Soetaert, K., Herman, P. M. J., Middelburg, J. J., Heip, C., Smith, C. L., Tett, P., and Wild-allen, K.: Numerical modelling of the shelf break ecosystem?: reproducing benthic and pelagic measurements, Deep Sea Res. Pt. II, 48, 3141–3177, 2001.

Soetaert, K., Hofmann, A. F., Middelburg, J. J., Meysman, F. J. R., and Greenwood, J.: The effect of biogeochemical processes on pH (Reprinted from Marine Chemistry, vol 105, pg 30–51, 2007), Mar. Chem., 106, 380–401, doi:10.1016/j.marchem.2007.06.008, 2007.

Sohma, A., Sekiguchi, Y., Kuwae, T., and Nakamura, Y.: A benthic-pelagic coupled ecosystem model to estimate the hypoxic estuary including tidal flat-Model description and validation of seasonal/daily dynamics, Ecol. Modell., 215, 10–39, doi:10.1016/j.ecolmodel.2008.02.027, 2008.

Stanev, E. V., He, Y., Staneva, J., and Yakushev, E.: Mixing in the Black Sea detected from the temporal and spatial variability of oxygen and sulfide – Argo float observations and numerical modelling, Biogeosciences, 11, 5707–5732, doi:10.5194/bg-11-5707-2014, 2014.

Tebo, B. M.: Manganese(II) oxidation in the suboxic zone of the Black Sea, Deep Sea Res. Pt., 38, S883–S905, doi:10.1016/S0198-0149(10)80015-9, 1991.

Tebo, B. M., Ghiorse, W. C., van Waasbergen, L. G., Siering, P. L., and Caspi, R.: Bacterially mediated mineral formation: Insights into manganese(II) oxidation from molecular genetic and biochemical studies, in: Geomicrobiology: Interactions Between Microbes and Minerals. The Mineralogical Society of America, Washington, D.C., 225–266, 1997.

Thorpe, S. A.: The Turbulent Ocean, Cambridge University Press, 2005.

UNESCO, Progress on oceanographic tables and standards 1983–1986: Work and recommendations of the UNESCO/SCOR/ICES/IAPSO Joint Panel. chap. 7.5: Oxygen solubility. UNESCO Technical Papers in Marine Science No. 50, 11 pp., 1986.

Umlauf, L., Burchard, H. and Bolding, K.: General ocean turbulence model, Source code documentation, Balt. Sea Res. Inst. Warn. Tech. Rep, 63, p. 346, 2005.

Van Cappellen, P. and Wang, Y. F.: Cycling of iron and manganese in surface sediments: A general theory for the coupled transport and reaction of carbon, oxygen, nitrogen, sulfur, iron, and manganese, Am. J. Sci., 296, 197–243, doi:10.2475/ajs.296.3.197, 1996.

Volkov, I. I.: Geokhimiya Sery v Osadkakh Okeana (Geochemistry of Sulfur in Ocean Sediments), Nauka, Moscow, 1984.

Wanninkhof, R.: Relationship between wind speed and gas exchange over the ocean revisited, Limnol. Oceanogr., 12, 351–362, doi:10.4319/lom.2014.12.351, 2014.

Wersin, P.: The Fe(II)-CO2-H2O system in anoxic natural waters: equilibria and surface chemistry, Swiss Fed. Inst. Technol., Dissertation ETH No.9230, 1990.

Wijsman, J. W. M., Herman, P. M. J., Middelburg, J. J., and Soetaert, K.: A Model for Early Diagenetic Processes in Sediments of the Continental Shelf of the Black Sea, Estuar. Coast. Shelf S., 54, 403–421, doi:10.1006/ecss.2000.0655, 2002.

Wolf-Gladrow, D. A., Zeebe, R. E., Klaas, C., Körtzinger, A., and Dickson, A. G.: Total alkalinity: The explicit conservative expression and its application to biogeochemical processes, Mar. Chem., 106, 287–300, doi:10.1016/j.marchem.2007.01.006, 2007.

Wollast, R.: Rate and mechanism of dissolution of carbonates in the system CaCO3-MgCO3, Aquatic chemical kinetics: reaction rates of processes in natural waters, Chemistry, in: Aquatic Chemical Kinetics: Reaction Rates of Processes in Natural Waters, edited by: Stumm, W., 431–445, 1990.

Yakushev, E.: RedOx Layer Model: A Tool for Analysis of the Water Column Oxic/Anoxic Interface Processes, in: Chemical Structure of Pelagic Redox Interfaces: Observation and Modeling, edited by: Yakushev, E. V. Springer-Verlag Berlin Heidelberg, 203–234, 2013.

Yakushev, E., Pakhomova, S., Sørenson, K., and Skei, J.: Importance of the different manganese species in the formation of water column redox zones: Observations and modeling, Mar. Chem., 117, 59–70, doi:10.1016/j.marchem.2009.09.007, 2009.

Yakushev, E. V and Neretin, L. N.: One-dimensional modeling of nitrogen and sulfur cycles in the aphotic zones of the Black and Arabian Seas, Global Biogeochem. Cy., 11, 401–414, doi:10.1029/97GB00782, 1997.

Yakushev, E. V., Pollehne, F., Jost, G., Kuznetsov, I., Schneider, B., and Umlauf, L.: Redox Layer Model (ROLM): A Tool for Analysis of the Water Column Oxic/anoxic Interface Processes, Warnemunde, 2006.

Yakushev, E. V., Pollehne, F., Jost, G., Kuznetsov, I., Schneider, B., and Umlauf, L.: Analysis of the water column oxic/anoxic inter-

face in the Black and Baltic seas with a numerical model, Mar. Chem., 107, 388–410, doi:10.1016/j.marchem.2007.06.003, 2007.

Yakushev, E. V., Chasovnikov, V. K., Murray, J. W., Pakhomova, S. V., Podymov, O. I., and Stunzhas, P. A.: Vertical hydrochemical structure of the black sea, Handb. Environ. Chem. Vol. 5 Water Pollut., 52007, 277–307, doi:10.1007/698_5_088, 2008.

Yakushev, E. V., Kuznetsov, I. S., Podymov, O. I., Burchard, H., Neumann, T., and Pollehne, F.: Modeling the influence of oxygenated inflows on the biogeochemical structure of the Gotland Sea, central Baltic Sea: Changes in the distribution of manganese, Comput. Geosci., 37, 398–409, doi:10.1016/j.cageo.2011.01.001, 2011.

Yakushev, E. V., Debolskaya, E. I., Kuznetsov, I. S., and Staalstrøm, A.: Modelling of the Meromictic Fjord Hunnbunn (Norway) with an Oxygen Depletion Model (OxyDep), edited by: Yakushev, E. V., Handb. Environ. Chem., July 2011, doi:10.1007/698_2011_110, 2013a.

Yakushev, E. V., Sorensen, K., and Sørensen, K.: On seasonal changes of the carbonate system in the Barents Sea: observations and modeling, Mar. Biol. Res., 9, 822–830, doi:10.1080/17451000.2013.775454, 2013b.

Yu, L., Fennel, K., Laurent, A., Murrell, M. C., and Lehrter, J. C.: Numerical analysis of the primary processes controlling oxygen dynamics on the Louisiana shelf, Biogeosciences, 12, 2063–2076, doi:10.5194/bg-12-2063-2015, 2015.

Zeebe, R. E. and Wolf-Gladrow, D.: CO_2 in Seawater, Equilibrium, Kinetics, Isotopes, Elsevier, 2001.